Geologica Acta, Vol.14, Nº 3, September 2016, 219-235
DOI: 10.1344/GeologicaActa2016.14.3.2

geologica acta

Genesis and petrology of Late Neoproterozoic pegmatites and aplites associated with the Taba metamorphic complex in southern Sinai, Egypt

K.M. ABDELFADIL[1] P.D. ASIMOW[2] M.K. AZER[2, 3*] H.A. GAHLAN[4,5]

[1]Geology Department, Sohag University
Sohag, Egypt

[2]Division of Geological & Planetary Sciences, California Institute of Technology
Pasadena, CA, USA

[3]Geological Sciences Department, National Research Centre
12622-Dokki, Cairo, Egypt Azer E-mail: mokhles72@yahoo.com

[4]Department of Geology and Geophysics, College of Science, King Saud University
Riyadh 11451, Saudi Arabia

[5]Geology Department, Assiut University
Assiut, Egypt

*Corresponding author

ABSTRACT

We present new field, petrographical, mineralogical and geochemical data from late Neoproterozoic pegmatites and aplites in southern Sinai, Egypt, at the northernmost limit of the Arabian-Nubian Shield. The pegmatites cross-cut host rocks in the Taba Metamorphic Complex (TMC) with sharp contacts and are divided into massive and zoned pegmatites. Massive pegmatites are the most common and form veins, dykes and masses of variable dimensions; strikes range mainly from E-W through NW-SE to N-S. Mineralogically, the massive pegmatites are divided into K-feldspar-rich and albite-rich groups. Zoned pegmatites occur as lenses of variable dimensions, featuring a quartz core, an intermediate zone rich in K-feldspars and an outer finer-grained zone rich in albite. All compositions are highly evolved and display geochemical characteristics of post-collisional A-type granites: high SiO_2, Na_2O+K_2O, FeO*/MgO, Ga/Al, Zr, Nb, Ga and Y alongside low CaO, MgO, Ba and Sr. They are rich in Rare Earth Elements (REE) and have extreme negative Eu anomalies (Eu/Eu*= 0.03–0.09). A genetic linkage between the pegmatites, aplites and alkali granite is confirmed by their common mild alkaline affinity and many other geochemical characteristics. These pegmatites and aplites represent the last small fraction of liquid remaining after extensive crystallization of granitic magma, injected along the foliation and into fractures of the host metamorphic rocks. The extensional tectonic regime and shallow depth of emplacement are consistent with a post-collisional environment.

KEYWORDS | **Arabian-Nubian shield. Sinai. Post-collisional. A-type rocks. Lithospheric delamination.**

INTRODUCTION

The basement rocks of Sinai, together with those of the eastern Desert of Egypt, constitute the northern extension of the Arabian-Nubian Shield (ANS) (Fig. 1 inset). This shield represents one of the largest tracts of Neoproterozoic juvenile continental on Earth crust (Patchett and Chase, 2002) and forms the northern segment of the East African Orogen (Stern, 1994). The shield evolved through several tectono-magmatic stages and represents a collage of juvenile volcanic arc terranes and associated ophiolite remnants, amalgamated during the assembly of Gondwana (*e.g.* Meert, 2003; Stoeser and Frost, 2006; Cox *et al.*, 2012). Post-collisional stabilization of the shield was followed by large-scale erosion and formation of a vast peneplain by Cambrian time (Bentor, 1985; Garfunkel, 1999; Avigad and Gvirtzman, 2009).

The Ern tip of the South Sinai, the northernmost corner of the ANS, is mainly occupied by juvenile crust and preserves rocks and structures associated with the pre-collisional, syn-collisional and post-collisional phases of the terminal assembly of the ANS (Eyal *et al.*, 2010, 2014; Be'eri-Shlevin *et al.*, 2011). The Sinai massif was uplifted during the late Neogene-Quaternary providing excellent fresh exposures of the late Neoproterozoic ANS (Fig. 1) (Bentor, 1985; Garfunkel, 2000; Eyal *et al.*, 2004).

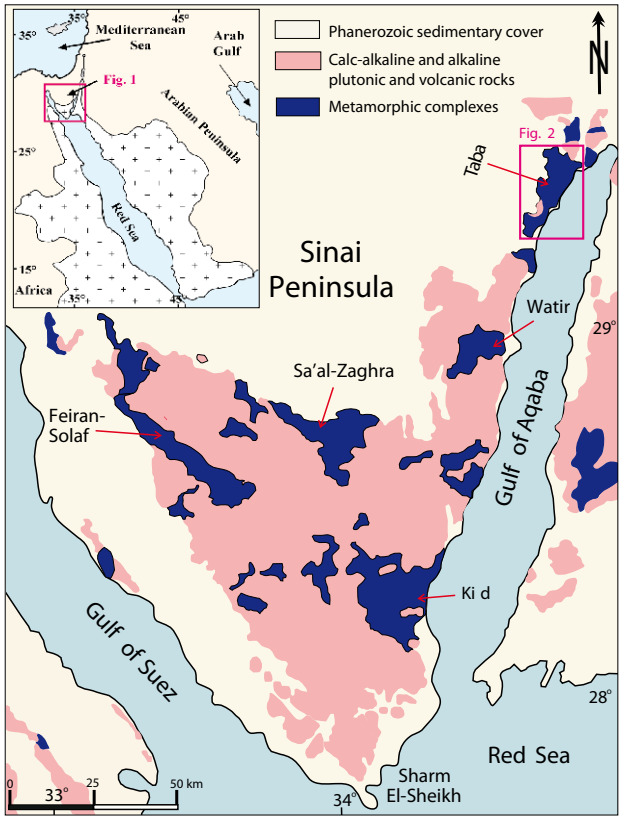

FIGURE 1. Geological map of Sinai (modified after Eyal *et al.*, 1980) with inset of ANS. Location of the study area displayed in Figure 2 is marked.

Pegmatites occur in a variety of shapes, sizes and geologic environments (see review in Dill, 2015). They are very coarse-grained crystalline rocks that, in places, contain giant crystals of feldspar, quartz or mica. Pegmatites have long drawn the attention of geologists high economic potential due to the concentration of rare elements and minerals often found in them and associated aplites (Dill, 2015). Pegmatites are present in various rock types of the northern ANS (*e.g.* Jackson, 1983; Abdalla and El-Afandy, 2003; Ghazaly *et al.*, 2015). In contrast to the pegmatites in the Eastern Desert of Egypt, those of the South Sinai have not been comprehensively surveyed. Most South Sinai pegmatites are found within the metamorphic complexes.

This study outlines the first detailed study of the pegmatites and aplites in the Taba Metamorphic Complex (TMC) in the northeast of South Sinai. Published reports of the Taba pegmatites are limited and make contradictory claims about their origin. El-Sheshtawi *et al.* (1988) considered the pegmatitic rocks around Wadi El-Morakh area (see Fig. 2) derived from within-plate magma, whereas Essawy *et al.* (1997) interpret the Taba pegmatites derived from syn-collisional melting of a crustal source during the late episode of the Pan-African orogeny. Here, we provide detailed field, petrographical, mineralogical and geochemical data the pegmatites and aplites, leading to a well-defined model of their tectonic history and tectono-magmatic evolution. We hope this work will encourage other researchers to study the pegmatites that occur in the basement rocks of Egypt, so that the economic significance of these rocks are better assessed.

GEOLOGIC OUTLINE

Regional geological setting

The late Neoproterozoic juvenile crust of the southern Sinai Peninsula is part of the northernmost sector of the ANS (Fig. 1). It was developed through three main successive phases including pre-collisional, syn-collisional and post-collisional (Eyal *et al.*, 2010, Be'eri-Shlevin *et al.*, 2011; Azer *et al.*, 2014). The pre-collisional phase (ca. 820–740Ma) is characterized by metamorphosed volcano-sedimentary rocks, gneisses and associated migmatites and amphibolites. The syn-collisional phase (ca. 670–630Ma) is characterized by variably deformed gabbro-diorite complexes, calc-alkaline granitoids and their volcanic equivalents. The post-collisional phase is represented by calc-alkaline (ca. 630–590Ma) and alkaline (ca. 610–580Ma) rock suites. The post-collisional calc-alkaline

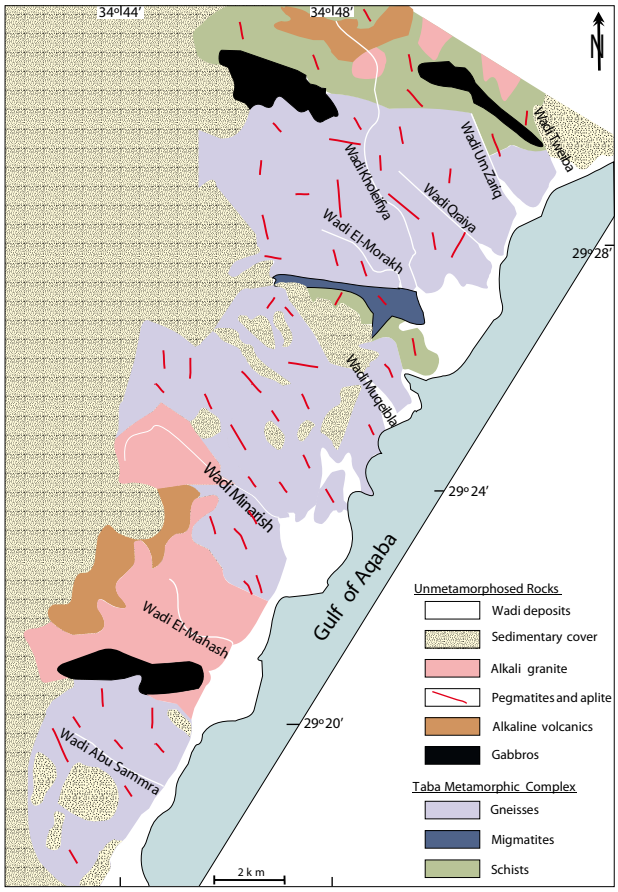

FIGURE 2. Geologic map of Taba area in southeast Sinai, Egypt (modified after Khalil *et al.*, 2015). See Figure 1 for location.

suite includes granitoids and Dokhan volcanics (Samuel *et al.*, 2001a, b; Azer and Farahat, 2011; Be'eri-Shlevin *et al.*, 2011), whereas the alkaline suite includes alkaline/peralkaline A-type granites and their volcanic equivalents (Azer, 2006; Samuel *et al.*, 2007; Eyal *et al.*, 2014). The end of calc-alkaline plutonic magmatism overlapped with the beginning of alkaline activity (Azer *et al.*, 2010; Eyal *et al.*, 2010; Be'eri-Shlevin *et al.*, 2011). According to Eyal *et al.* (2014), post-collisional magmatism started at 635Ma in northeast South Sinai, and at a younger age (~610Ma) in the southeast of South Sinai. This indicates that the closure of the Mozambique Ocean propagated from northeast South Sinai towards the southeast over about 25Ma.

One of the most striking features of South Sinai is the abundance of post-collisional plutons and associated volcano-sedimentary sequences, whereas older rocks, now comprising parts of metamorphic complexes, are scarce, and ophiolites are completely absent (*e.g.* Bentor, 1985; Stein, 2003; Azer and El- Gharbawy, 2011). Five metamorphic complexes (Feiran-Sulaf, Sa'al-Zaghra, Kid, Watir and Taba) are exposed within the Precambrian basement of Sinai, Egypt. In addition, many smaller areas of metamorphic rocks are scattered throughout the Sinai massif. The pegmatitic rocks, the target of the present work, are located in the TMC (Fig. 1).

Geology of Taba area

The TMC is exposed along the western side of the Gulf of Aqaba and in the northeast of South Sinai (Fig. 1). It is elongated in a NE-SW direction, about 35km long and 7km wide. The metamorphic rocks of the TMC in the Taba area consist of metapelitic schists, migmatites and gneisses. The grade of metamorphism ranges from greenschist to amphibolite facies. They are intruded by unmetamorphosed post-collisional rocks (alkali granites, gabbros and volcanics) and to the west unconformably overlain by Phanerozoic sediments (Fig. 2). (Eyal, 1980; Eyal and Amit, 1984; Abu El-Enen *et al.*, 1999, 2004).

The schists represent the oldest rock unit in the mapped area. They crop out at Wadi Tweiba and Wadi El-Morakh and are mainly biotite schists and garnet biotite schists. The schists are moderately coarse grained and have a greater proportion of granular (quartz and feldspar) constituents than the gneisses. They are intruded by gabbros and alkali granite. Near the mouth of Wadi El-Morakh, they are highly migmatized and segregated parallel to foliation into thin veins and lenses of granitic leucosome and metamorphic host rock. The migmatites exhibit a variety of textures such as agmatitic structure, surreitic texture and boudinage.

The gneisses are the most common rock type in the mapped area. They are medium to coarse grained and display very strongly lineated, weakly to highly foliated gneissic structures and prominent augen. The absence of relic bedding or other sedimentary structures in the gneisses indicate their orthogneiss character, supported by the presence of off-shoots and apophyses of gneiss in the schists and the presence of schist xenoliths and mafic enclaves within the gneisses. The gneisses range in composition from tonalitic to granitic (Eyal, 1980; Abu El-Enen *et al.*, 1999). In the southern part of the TMC, the gneisses are less deformed and more felsic than in the northern part. The protoliths of the orthogneisses are calc-alkaline arc granitoids that were emplaced along an active continental margin during the pre- to syn-collision stage of the Pan-African Orogeny (Abu El-Enen *et al.*, 1999).

The post-collisional rocks in the mapped area include mafic intrusions, alkali granites and volcanics (Abu El-Enen, 2000; Samuel *et al.*, 2007; Abdel-Karim, 2013; Khalil *et al.*, 2015). The mafic intrusions include the Wadi El-Mahash and Wadi Tweiba gabbroic rocks. They are unmetamorphosed and assigned to post-collisional magmatism (Abdel-Karim, 2013; Khalil *et al.*, 2015).

Khalil *et al.* (2015) attributed the subduction-related geochemical characteristics of the gabbro of Wadi El-Mahash to the partial melting of lithospheric mantle source enriched during the early subduction beneath the ANS. On the other hand, mapping further north had led Israeli geologists to consider that the Wadi El-Mahash and Wadi Tweiba mafic intrusions correlate with greenschist-grade Shahmon metabasite (Shimron, 1972; Eyal *et al.*, 2014).

Alkali granites are exposed in the northern and southern parts of the TMC. They stand as high, irregular crescent-shaped outcrops against the country rocks and several apophyses of the alkali granite extend into the country rocks. A conspicuous feature of the alkali granites is an absence of mafic microgranular enclaves or dykes. They have typical characteristics of an intra-plate tectonic setting (Abu El-Enen, 2000). The correlative volcanic rocks in the mapped area are well exposed along Wadi Kholeifiya and Wadi El-Mahash. They are mainly alkaline rhyolites and their pyroclastics with minor trachyte and trachyandesite (Samuel *et al.*, 2007); the volcanic sequence is also consistent with their emplacement in an intra-plate tectonic setting.

Pegmatites are widely distributed in the gneisses and schists of the TMC and less common in the gabbros and, as pockets, in the alkali granites. Their light color contrasts clearly with the darker surrounding rocks. Their lengths vary from a few meters up to 1km and their widths from a few centimeters to a few meters. Most of the pegmatite dikes have NW-SE, E-W and N-S trends. Some pegmatite bodies show miarolitic cavities. Based on field observations, the pegmatites can be divided into massive pegmatites and zoned pegmatites; the massive variety are the most common. Massive pegmatites occur in the form of large and small veins and dykes as well as small bodies of variable dimensions and trends. The zoned pegmatites are rare and are found only near intrusive bodies of alkali granite. They are represented by lenses of variable dimensions featuring a thin rim enriched in sodium feldspar, a broad intermediate zone of potassium feldspar, and, frequently, a quartz core (Fig. 3).

The pegmatites associated with the schists are mostly concordant with the bedding planes and some of them are cataclastic to variable degrees. A few bodies of pegmatite are affected by strike-slip faults and have signs of mylonitization. These features indicate emplacement of pegmatitic masses both before and after fault movement in the study area. At the entrance of Wadi El-Morakh, a few roof pendants of schist and gneiss are observed in the peripheral parts of the pegmatite masses. The foliation planes of schists and gneisses in the roof pendants differ in orientation from

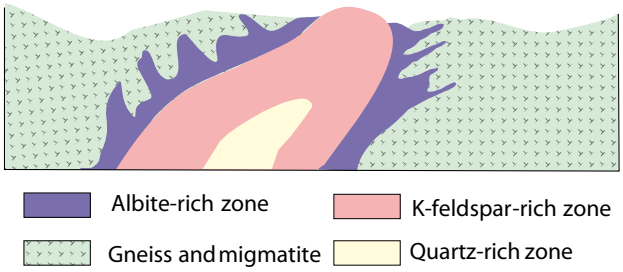

FIGURE 3. Sketch showing the different zones in the zoned pegmatites.

the regional fabric and indicate rotation of the roof pendants during transport with the pegmatitic magma. A few pegmatite lenses display an obvious thin hybrid zone due to metasomatic reaction between the pegmatite material and the host rocks. Rare quartz pegmatites are observed in a few locations in the TMC.

Aplites are observed in a few localities in the TMC, especially in its northern part. Aplites occur as veins as well as low-angle to subhorizontal sheet-like sills with granitic compositions. Aplites also occur as marginal selvages within pegmatites. Scattered large crystals of alkali feldspars are present in the some of the aplites.

Age constraints for the Taba rocks

The age and petrogenesis of the metamorphic rocks exposed in the Taba area have been the basis of much controversy (Stern and Manton, 1987; Shimron, 1988; Eyal *et al.*, 1991; Cosca *et al.*, 1999; Morag *et al.*, 2011). U-Pb dating of detrital zircons from the northern part of the TMC near Eilat yield ages of 820–800Ma (Jarrar *et al.*, 1983; Kröner *et al.*, 1990). However, recent SIMS U-Pb dating of detrital zircons revealed ages spanning a much wider range, between 870 and 790Ma, with a major peak at ca. 820Ma (Eyal *et al.*, 2014).

On the basis of low initial $^{87}Sr/^{86}Sr$ ratios (0.7035±5) and positive $\varepsilon_{Nd}(t)$ values (+4) of schists exposed in the northern part of the TMC near Eilat, it appears that these rocks were derived from an island arc rather than a preexisting continental crust (Bielski, 1982; Kröner *et al.*, 1990; Stein and Goldstein, 1996; Cosca *et al.*, 1999). An island arc source is supported also by juvenile $\varepsilon_{H}f(t)$ for individual dated zircons (Morag *et al.*, 2011), the limited range of detrital zircon ages (870–790Ma) and the scarcity of detrital zircons with ages older than the oldest ophiolites of the ANS (ca. 870Ma; Pallister *et al.*, 1988; Ali *et al.*, 2010). The age of the sedimentation of the protolith of the Taba schist is constrained by the youngest arc-related plutonic activity intruding the schist, beginning at ca.790–780Ma (Kröner *et al.*, 1990; Morag *et al.*, 2011) with the intrusion

of the tonalitic to quartz-dioritic protolith of the Taba gneiss. Kröner *et al.* (1990) obtained a somewhat younger single zircon age for the Eilat granitic gneiss (744±5Ma).

The mafic plutons exposed in the mapped area (Wadi Tweiba and Wadi El-Mahash) yielded single zircon U-Pb ages between 670 and 612Ma (Kröner *et al.*, 1990; Morag *et al.*, 2011). The 612Ma is an acceptable age because these mafic plutons are unmetamophosed, post-collisional members of the complex (Abdel-Karim, 2013; Khalil *et al.*, 2015). Eyal et al (2014) correlated the mafic intrusions of Wadi El-Mahash and Wadi Tweiba to the 660–670Ma Shahmon metabasite in southern Israel, which is intruded by ca. 659Ma granitic gneiss dikes (Eyal *et al.*, 1991) and by the ca. 630Ma undeformed Rehavam granitic pluton (Be'eri-Shlevin *et al.*, 2009; Morag *et al.*, 2011). The most straightforward interpretation of these zircon ages is that the mafic plutons in the mapped area are different from and younger than the Shahmon metabasite. They represent a postcollisional stage of plutonic activity (630–635Ma; Be'eri-Shlevin *et al.*, 2009) that later experienced penetrative ductile deformation prior to intrusion of the alkali granites of Wadi El-Mahash.

SAMPLING AND ANALYTICAL METHODS

A total of 55 large samples (~2kg) were collected in order to optimize representation of these coarse grained rocks. We selected the simple massive pegmatites, devoid of any visible zonation, and aplitic samples devoid of feldspar megacrysts for chemical analyses. Concentrations of major and trace elements were determined by X-Ray Fluorescence (XRF) (ThermoARL XRF Spectromemter) at the GeoAnalytical Lab, Washington State University. The analytical precision for XRF analyses, as calculated from duplicate samples, is better than 1% for most major elements and better than 5% for most trace elements. The Rare Earth Elements (REE) for eight representative whole-rock samples were determined by solution-source Inductively Coupled Plasma Mass Spectrometry (ICP-MS) at the ACME Analytical Laboratories, Vancouver, Canada.

The chemical compositions of essential minerals were analized in the USA and France. Minerals in polished sections were analyzed by electron probe micro-analyzer (JEOL JXA-8200) at the GPS Division Analytical Facility, California Institute of Technology. The analytical conditions were 15kV accelerating voltage, 25nA beam current, and a focused beam (<1μm). Some minerals in the thin-polished sections were also analyzed using a CAMECA CAMEBAX SX-50 Electron Probe Micro Analyzer (EPMA) housed at the BRGM, Orléans, France, at 15kV accelerating voltage and 20nA beam current. Various natural and synthetic mineral standards were used in both laboratories.

PETROGRAPHY

Country rocks

Schists are composed mainly of oligoclase, quartz and biotite with smaller amounts of muscovite, garnet, andalusite, sillimanite, staurolite and cordierite. The pelitic schist layers are richer in biotite whereas psammitic layers are enriched in quartz. The accessory minerals include zircon, apatite and opaques. The gneisses range in composition from quartz-dioritic to granitic. They consist of plagioclase, quartz, biotite and amphiboles in variable proportions, prominent K-feldspar and garnet porphyroblasts, and accessory zircon, apatite, titanite and opaques. Based on the mineralogical compositions, the metamorphic grades of TMC range from lower-greenschist to amphibolite facies with a general increase of grade towards the schists. Greenschist facies in both schists and gneisses is characterized by biotite and small garnet crystals, whereas amphibolite facies is characterized by porphyroblasts of garnet, staurolite, cordierite, andalusite and sillimanite.

The granites of the TMC vary in composition from syenogranites to alkali granites. All the granites consist essentially of K-feldspar, quartz, plagioclase, biotite and hornblende in variable amounts. The main petrographic feature of the granites is the decrease in modal abundance of plagioclase and hornblende from syenogranites to alkali granites. Apatite, titanite, zircon and iron oxides are accessories. Graphic textures of quartz and K-feldspars are common, especially in the alkali granites. There are many textural and mineralogical similarities between the alkali granites and the pegmatites in the mapped area but the alkali granites have more plagioclase and less quartz than the pegmatites.

Pegmatites

There are various classifications of pegmatites based on their mode of occurrence, internal structure and mineralogical composition. The studied pegmatites show variable internal structures, grain size variation, textural patterns and mineral compositions that systematically and progressively change across the pegmatitic bodies. On the basis of mineralogy, the studied pegmatites are classified as granitic. Based on the internal structures, the pegmatites are distinguished into zoned and unzoned (massive) pegmatites. The massive pegmatites are divided into K-feldspar rich (K-rich) and albite rich (Na-rich) pegmatites.

K-feldspar rich pegmatites are very coarse-grained rocks and consist mainly of quartz, microcline-perthite, orthoclase, muscovite, and small amounts of albite and biotite. Iron oxides, zircon, fluorite and apatite are accessories. Secondary minerals include sericite, epidote, and chlorite. Potassium feldspar occurs as coarse-grained, subhedral to anhedral prismatic crystals. Microcline crystals show tartan twinning and are usually intergrown with albite, forming patchy perthite (Fig. 4A). Some large crystals of orthoclase enclose small crystals of albite (Fig. 4B) and/or iron oxides and zircon. Quartz shows undulatory extinction. The margins of some of the larger feldspar and quartz grains are surrounded by a narrow zone of fine-grained recrystallized quartz, feldspar, and muscovite that forms a mortar structure. Very fine-grained muscovite occurs as aggregates along the borders of feldspar grains; such mica may be deuteric. In some places the pegmatites altered the metamorphic country rocks at their contacts by the introduction of albite, tourmaline, muscovite and apatite.

The albite rich pegmatites are medium- to coarse-grained rocks and consist of albite, quartz, K-feldspar, biotite and muscovite. Opaques, allanite and zircon are accessory minerals. Albite occurs as euhedral to anhedral prismatic crystals characterized by lamellar twinning (Fig. 4C). Some albite crystals have bent and broken twin planes. Quartz may be graphically intergrown with albite (Fig. 4D) or contain small inclusions of rounded to euhedral albite. Sometimes, the quartz forms veinlets or is distributed along contacts of other minerals. Muscovite occurs as inclusions within the feldspars or as aggregates around them (Fig. 4E). Rare skeletal tourmaline crystals are intimately intergrown with and embayed by quartz and albite or appear as embayed inclusions in albite. These inclusions with embayed borders indicate that the tourmaline was an early-crystallizing phase. Nevertheless, the intimate intergrowths indicate that tourmaline was largely contemporaneous with quartz and albite.

Thin sections from the thin albite-rich border and broad K-rich core zones of a large zoned pegmatite lens were examined. The border zone consists mainly of albite, K-feldspar, microcline, microcline-perthite, and a small amount of quartz and biotite. Rare amphibole, muscovite, and tourmaline are observed in the outer zone. Also, the outer zone of some zoned pegmatites trapped crystals of beryl with c-axis and elongation normal to the pegmatite contact (Fig. 4F). This is may be due to the metasomatic interaction between pegmatites and their host rocks. The core zone is composed mainly of quartz, microcline-perthite, muscovite and a small amount of biotite and albite. The accessory minerals in the zoned pegmatites include iron oxides, apatite and zircon, whereas sericite and epidote occur as secondary minerals. Both albite and quartz in the border and core zones have strain shadows, but albite was more susceptible to deformation than quartz.

Pegmatitic quartz is very rare and found only along Wadi Tweiba at the northern end of the TMC. It is coarse-grained and consists mainly of quartz. Milky quartz is most abundant, with rare smoky quartz. Also, opal or chalcedony is observed in the outer margins of the quartz pegmatite due to supergene alteration.

Aplites

Aplites are uniformly fine-grained with allotriomorphic texture. They consist chiefly of quartz and albite with subordinate K-feldspars and biotite in variable quantities. The accessory minerals include opaques, garnet, zircon and muscovite. A few samples contain large crystals of K-feldspars or plagioclase. In some occurrences these large crystals are replaced by sugary aggregates of albite. The K-feldspars include orthoclase and microcline. Skeletal crystals of quartz and feldspar along with graphic intergrowth of quartz and feldspars are common in the aplites. These textures indicate rapid crystal growth rates.

MINERAL CHEMISTRY

Chemistry of the major and some accessory minerals from the massive pegmatites and aplites were analyzed by Electron Probe Microanalyzer. The full dataset of mineral chemistry is given in the online version (Tables I-VII Electronic Appendix, available at www.geologica-acta.com).

The chemical composition, structural formulae and end-member components of the analyzed feldspars, both alkali feldspars and plagioclases, are given in Tables I and VI according to the compositional nomenclature given by Deer *et al.* (1992). The alkali feldspars in the studied rocks are orthoclase, while the plagioclases include albite and oligoclase. Microcline would also be called orthoclase in this nomenclature. Orthoclase in the K-rich pegmatite ranges in composition from $Or_{89.3}$ to $Or_{98.4}$ with an average of $Or_{95.3}$, whereas those in the Na-rich pegmatite range from $Or_{91.6}$ to $Or_{95.3}$ with an average of $Or_{93.2}$. The orthoclase in the aplites shows variation in composition ranging from $Or_{85.4}$ to $Or_{89.7}$ with an average of $Or_{88.1}$. The albites in all the different rock types are rather similar in composition, having very low anorthite content ($An_{0.0\text{-}2.6}$). Oligoclases were analyzed in K-rich pegmatite ($An_{11.4\text{-}14.9}$), Na-rich pegmatite ($An_{13.7\text{-}15.1}$) and aplites ($An_{19.3\text{-}22.7}$).

Selected biotite crystals were analyzed in Na-rich pegmatite and aplites. Chemical compositions and structural formulae of the biotite are given in Table VII. The analyzed biotite crystals are substantially richer in $FeO_{(t)}$ (18.38–29.88wt.%) than MgO (5.12–9.73wt.%). The

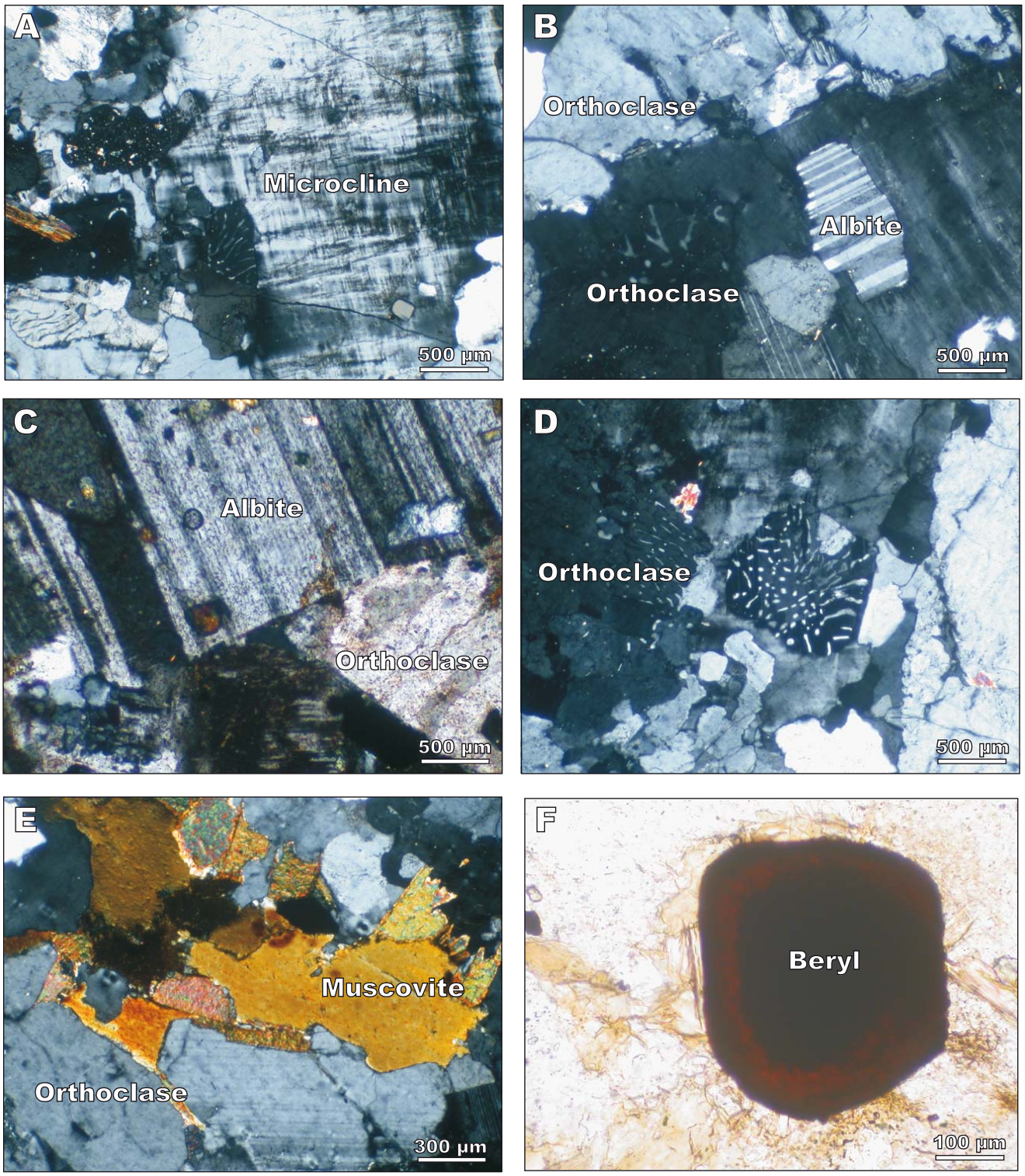

FIGURE 4. Textural variation among Taba pegmatites. All photomicrographs in cross-polarized light, except F in plane light. A) Microcline crystals show tartan twinning and intergrowths with albite forming patchy perthite in the K- rich pegmatite. B) Some large crystals of orthoclase enclose small crystals of albite in the K -rich pegmatite. C) Euhedral prismatic albite crystal in the Na-rich pegmatite. D) Quartz graphically intergrown with albite. E) Muscovite aggregates among feldspar crystals in the Na-rich pegmatite. F) Beryl crystal in the zoned pegmatite.

composition and texture of biotites indicate that they are primary igneous phases in all samples. This is supported by plotting the chemical analyses of biotites on the TiO_2–$FeO_{(t)}$–MgO ternary diagram of Nachit *et al.* (2005); on this diagram they show the chemical characteristics associated with primary igneous biotites (Fig. 5). The iron-rich composition of the studied biotites is similar to those of post-collisional suites in south Sinai (Farahat and Azer, 2011).

WHOLE ROCK CHEMISTRY

The analyzed samples were carefully selected to avoid cross cutting veinlets and/or carbonate-filled fractures. Eighteen samples of pegmatites and aplites (12 massive pegmatites and 6 aplites) were selected for chemical analysis (Table 1). Also, five alkali granite samples were analyzed to compare and complete the picture of the relationship between the pegmatites, aplites and alkali granites. Major element and trace element, including REE, concentrations are used here to typify the distinct geochemical characteristics of the rock types already distinguished by field relations and petrography.

A number of classification schemes for pegmatites have been suggested, based on various combinations of emplacement depth, mineralogical or chemical composition, metamorphic grade and minor element content (Černý, 1991; Wise, 1999; Ercit, 2004; Černý and Ercit, 2005). The standard composition-based categories divide pegmatites into granitic, syenitic and gabbroic groups; among these, granitic pegmatites are the most abundant (London, 2008). On the basis of mineralogy, the studied pegmatites and aplites are all classified as granitic and the geochemical data discussed below support a consistent assignment into the granitic pegmatite class. Granitic pegmatites can be further divided into various types and subtypes depending on the presence of accessory minerals and metals. Pegmatites with especially low REE content are classified as miarolitic pegmatites.

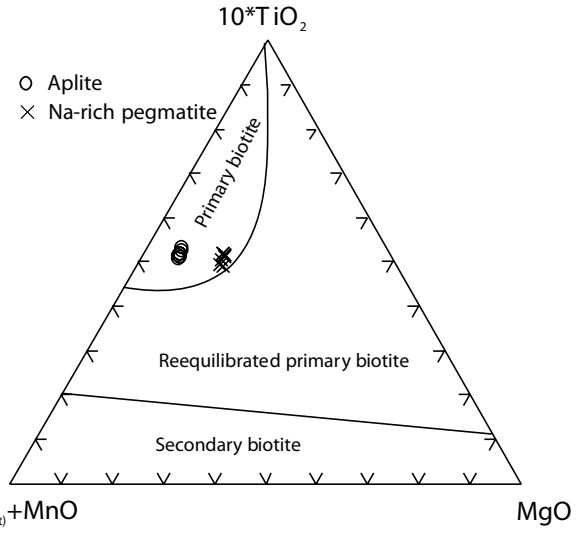

FIGURE 5. TiO2-FeO(t)-MgO ternary diagram for biotite classification (Nachit *et al.*, 2005).

Although all the studied rocks are high-silica felsic rock, there are significant variations in silica content. Aplites have the highest silica content (76.07–77.01wt.% SiO_2), followed by pegmatites (73.02 to 75.12wt.% SiO_2) and then alkali granites (73.2–74.14wt.% SiO_2). The Na-rich pegmatite, defined by high albite modal abundance, is in fact richer in Na_2O ($Na_2O/K_2O>1.17$) than the K-rich pegmatite defined by high orthoclase abundance ($Na_2O/K_2O<0.98$). The Aplites are markedly sodic in composition ($Na_2O/K_2O>1.03$). The leucocratic character of the pegmatites, aplites and alkali granites is clear from their CIPW norms, with light minerals (quartz, orthoclase and albite) greater than 91% in all samples. The normative anorthite content in the pegmatites and aplites are <5.06%, consistent with the sodic feldspar compositions observed in the microprobe analysis. The Alumina Saturation Index [ASI, molar ratio $Al_2O_3/(Na_2O+K_2O+CaO)$] of all studied samples is near unity (Table 1). On the R_1-R_2 discrimination diagram of De la Roche *et al.* (1980), the pegmatite and alkali granites samples plot in the granite field, whereas aplites plot in the alkali granite field (Fig. 6A).

The high agpaitic index (AI= (Na + K)/Al on a molecular basis) of the pegmatites (AI=0.86–0.90), aplites (AI= 0.90–0.96) and alkali granites (AI= 0.86–0.88) indicate an alkaline nature (Liégeois and Black, 1987; Liégeois *et al.*, 1998). However, all the samples plot in the "highly fractionated calc-alkaline" field on the Sylvester (1989) diagram (Fig. 6B). The slightly lower AI for alkali granite indicates it is less evolved than the pegmatites and aplites. Whalen *et al.* (1987) suggested the use of Ga/Al *versus* certain major and trace elements to distinguish between A-type granites and other granites (M-, I- and S-type). Most of the analyzed samples have high Ga/Al and plot consistently in the A-type granite field on the Ga/Al *vs.* $FeO_{(t)}/MgO$ diagram of Whalen *et al.* (1987; Fig. 6C). It should be noted that highly fractionated felsic I-type granites can have Ga/Al ratios and some major and trace element values that overlap those of typical A-type granites (Whalen *et al.*, 1987). Hence, it is possible that the A-type characteristics of the studied rocks might be explained by extreme fractionation from calc-alkaline magmas.

The REE concentrations in the pegmatites, aplites and alkali granites are listed in Table 2. They are normalized to chondrite values of Evensen *et al.* (1978) and are presented in Figure (7A). The K-rich pegmatites are richer in REE (310–358ppm) than the Na-rich pegmatites (211–214ppm), aplites (179–186ppm) and alkali granites (203–262ppm). The REE patterns of all the rock types are enriched in the LREE

TABLE 1. Chemical composition of pegmatites, aplites and granite of Taba Metamorphic Complex

Rock type	Pegmatite												Aplite						Granite				
	K-rich pegmatite					Na-rich pegmatite																	
Sample	PT22	PT25	PT34	PT4	PT7	PT1	PT10	PT13	PT16	PT28	PT37	PT41	AT14	AT21	AT26	AT3	AT30	AT38	GT1	GT10	GT13	GT4	GT7
Major oxides (wt.%)																							
SiO_2	74,4	73,2	74,9	75,1	73,7	73,3	73	74,4	73,3	73,4	73	73,1	76,6	76,1	76,8	76,6	77	76,2	73,3	73,4	72,9	74,1	73,2
TiO_2	0,09	0,1	0,12	0,08	0,12	0,14	0,07	0,08	0,11	0,08	0,12	0,09	0,05	0,08	0,07	0,07	0,06	0,09	0,14	0,16	0,18	0,14	0,15
Al_2O_3	14,1	14,6	14	13,4	14	14,6	14,5	14,1	14,2	14,2	14	14,6	12,8	13	12,5	12,6	12,6	13,1	13,9	13,9	13,9	13,9	14
Fe_2O_3	1,09	1,22	0,92	1,25	1,19	1,17	1,84	0,98	1,15	1,19	1,01	1,27	0,78	0,92	0,82	0,87	0,79	1,05	1,33	1,38	1,61	1,58	1,43
MnO	0,03	0,03	0,01	0,01	0,05	0,05	0,09	0,02	0,03	0,02	0,03	0,08	0,03	0,06	0,04	0,02	0,02	0,08	0,02	0,02	0,03	0,03	0,02
MgO	0,16	0,19	0,14	0,09	0,15	0,12	0,1	0,13	0,21	0,27	0,25	0,13	0,06	0,09	0,1	0,08	0,09	0,11	0,26	0,23	0,22	0,19	0,27
CaO	1,11	1,04	1,02	0,93	1,08	1,05	0,92	0,98	1,12	1,18	1,07	0,94	0,36	0,56	0,44	0,48	0,41	0,64	1,21	1,36	1,45	1,37	1,41
Na_2O	4,38	4,43	4,41	4,07	4,39	5,09	5,34	5,05	4,87	4,76	4,92	5,29	4,57	5,02	4,45	4,59	4,29	5,05	4,48	4,32	4,35	4,35	4,41
K_2O	4,62	5,03	4,52	4,38	4,57	4,21	3,98	3,84	3,94	4,07	3,98	3,78	4,31	3,79	4,32	3,99	3,94	3,55	4,49	4,53	4,45	4,43	4,43
P_2O_5	0,04	0,04	0,05	0,03	0,07	0,06	0,09	0,04	0,08	0,03	0,08	0,08	0,05	0,04	0,03	0,02	0,04	0,03	0,09	0,08	0,11	0,06	0,07
LOI	0,32	0,44	0,37	0,27	0,69	0,31	0,35	0,25	0,42	0,35	0,77	0,73	0,35	0,52	0,41	0,25	0,31	0,28	0,66	0,58	0,74	0,51	0,68
Total	100	100	100	99,6	100	100	100	99,8	99,4	99,5	99,3	100	100	100	100	99,5	99,5	100	99,9	100	99,9	101	100
Trace elements (ppm)																							
Rb	157	163	178	144	201	112	101	91	103	69	64	106	124	145	104	97	131	152	166	169	183	182	170
Sr	131	122	111	123	94	103	87	116	97	108	102	89	25	43	43	41	26	61	154	126	147	139	148
Ba	153	145	184	149	107	164	185	172	164	237	183	159	127	134	155	150	138	142	388	374	424	356	401
Nb	11,1	13,2	13,9	16,1	22,6	16,5	21,2	12,4	14,8	12,4	11,3	17,5	19,5	22,7	24,4	18,5	22,2	25,5	18,6	17,1	16,3	19,8	14,7
Th	13	12	12	9	14	8	11	14	9	13	10	8	9	13	11	14	12	10	16	16	16	17	15
U	5	4	8	6	7	4	5	7	6	3	5	5	4	5	7	5	6	5	4	4	5	6	4
Zn	27	30	24	32	11	11	10	18	26	22	21	17	22	18	29	24	26	23	17	15	17	13	16
Zr	117	120	89	100	119	89	96	105	111	101	94	121	135	149	142	141	137	150	211	216	243	244	214
Y	29	33	28	30	33	29	28	32	29	31	22	29	37	40	39	38	43	36	34	36	32	35	34
La	15	17	19	20	26	24	29	21	15	23	18	28	29	35	26	23	33	35	18	20	19	22	21
Ce	6		4	3	4	2	4	5	6	5	4	2	2	1	3	1	2	4	6	7	9	5	8
Pr	3	2	1	2	3	2	1	3	2	3	4	4	0	1	1	2	0	2	6	6	8	4	7
Nd	7	6	7	6	7	5	7	5	8	9	10	8	6	5	7	8	7	6	18	17	18	15	16
Eu	2	1	5	3	4	1	4	3	5	4	2	5	3	1	2	4	3	2	8	7	10	6	8
Sn	15	18	26	16	42	18	24	21	18	16	23	37	26	32	24	27	23	29	42	37	52	45	57
Hf	1	2	2	1	3	3	2	2	3	3	3	4	0	1	2	1	0	1	1	2	5	4	3
CI*	2,16	2,37	1,75	2,14	2,27	2,29	3,21	1,95	2,33	2,71	2,44	2,38	1,38	1,95	1,79	1,71	1,46	2,07	3,07	3,15	3,7	3,31	3,36
DI**	92,7	92,6	93,3	93	92,6	93,1	92,7	93,6	92,3	92	93	92,9	96,9	96,1	96,7	96,3	96	95,2	92,1	91,4	90,9	91,1	91,1

* Colour Index

** Differentiation Index

relative to HREE [(La/Lu)n= 2.620-12.960]. It is clear that the REE of each type are generally similar and show smooth patterns from LREE to HREE interrupted by characteristic negative Eu-anomalies. Negative Eu-anomalies are most prominent in pegmatites (0.03–0.08), followed by aplites (0.08–0.09) and alkali granites (0.36–0.38).

The differences in the REE patterns among samples and rock types reflect, most probably, the nature of the crystallizing accessory mineral phases. The extremely negative Eu-anomalies of pegmatites and aplites (0.03–0.09) can be attributed to extended fractional crystallization of feldspars and to melt-fluid interaction in the last stages of magma solidification (Jahn *et al.*, 2001; Zhao *et al.*, 2002, Lee *et al.*, 2013).

DISCUSSION

Geotectonic affinities

Previous studies dealing with the tectonic model of the Taba pegmatites are mutually inconsistent. The tectonic settings proposed for the Taba pegmatites include both within-plate and syn-collision settings (El-Sheshtawi *et al.*, 1988; Essawy *et al.*, 1997). These ideas have remained untested due to the lack of detailed field work, mineralogical observations and geochemical data. Our results, however, allow us to confidently define the tectonic setting of the Taba pegmatites and their associated rocks (alkali granites and aplites). Field investigations clearly demonstrate that the Taba pegmatites cut the late Pan-African gneisses and schists, postdating the regional metamorphism of their host rocks. Nonetheless, there is some evidence of post-magmatic deformation of all the varieties of pegmatite: quartz undulatory extinction in the K-rich massive pegmatite, broken and bent plagioclase twin planes in the Na-rich massive pegmatite, and strain shadows in the outer and border zones of the zoned pegmatites.

The overall chemical characteristics of the Taba pegmatites, aplites and alkali granites are consistent with a post-collisional tectonic setting. In the original Rb vs. Y+Nb tectonic discrimination diagram of Pearce *et al.* (1984), the analyzed samples plot in the overlap area between volcanic-arc and within-plate fields (Fig. 7B),

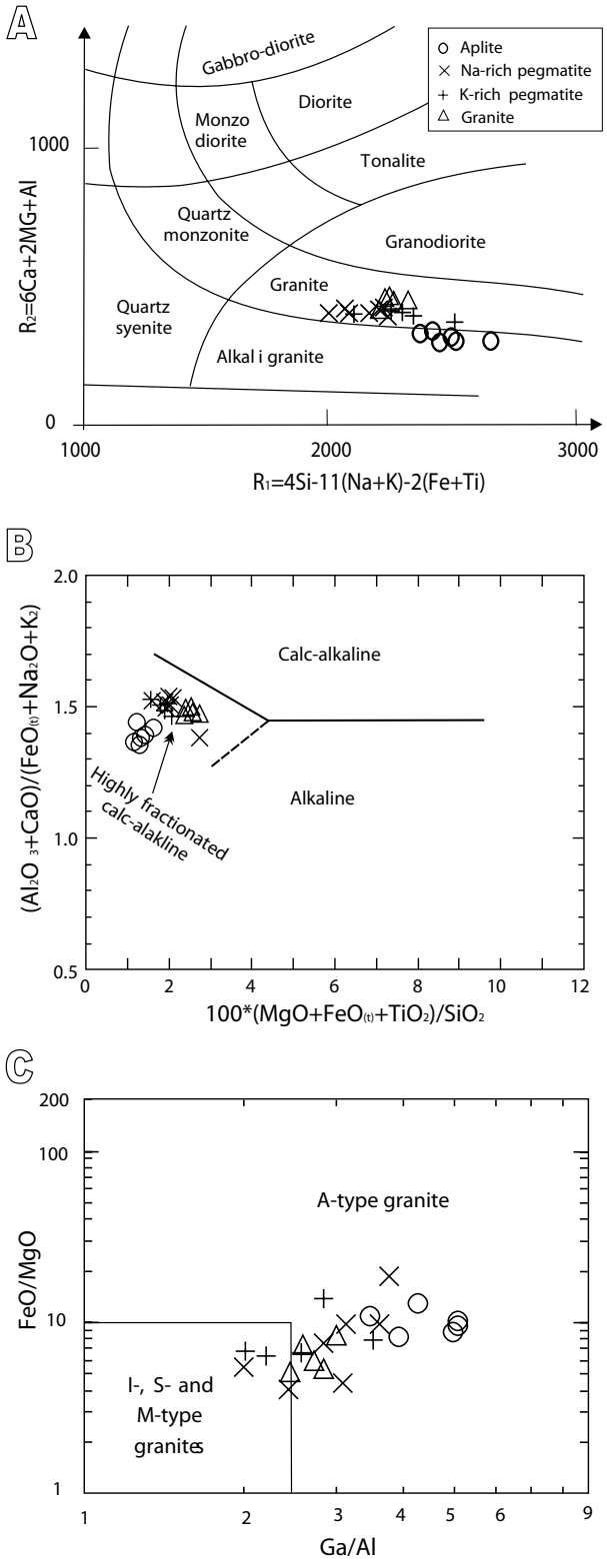

FIGURE 6. A) Nomenclature of igneous rocks using the R_1-R_2 discrimination diagram (De la Roche *et al.*, 1980). B) $(Al_2O_3+CaO)/(FeO_{(T)}+Na_2O+K_2O)$ *versus* $100(MgO+FeO_{(T)}+TiO_2)/SiO_2$ diagram for distinguishing between calc-alkaline, highly fractionated calc-alkaline granites and alkaline granites (Sylvester, 1989). C) Ga/Al *vs.* $FeO_{(t)}$/MgO diagram of Whalen *et al.* (1987).

within in the field later identified as post-collisional by Pearce (1996). The post-collisional setting is supported by using the SiO_2 *vs.* Al_2O_3 discrimination diagram of Maniar and Piccoli (1989) (Fig. 7C).

Eyal *et al*. (2010) discussed geology, geochemistry and isotope data of post-collisional calc-alkaline and alkaline-peralkaline granites of the Sinai Peninsula (Egypt) and southern Israel. Here we compared the REE data of the present study with calc-alkaline and alkaline granitoids of post-collisional setting (Eyal *et al*., 2010; Azer, 2013; Sherif *et al*., 2013; Azer *et al*., 2014). It is evident that the studied rocks have chondrite normalized REE patterns very similar to those of other post-collisional alkaline plutons, including the large magnitude of the prominent Eu negative anomaly (Fig.7A).

Magma source and petrogenesis

In the 1970s and 80s, the most widely accepted model of pegmatite genesis invoked a process of fractional crystallization of granitic melt (Jahns and Burnham, 1969). It has, however, also been proposed that it may be possible to form them by direct anatexis of metamorphic rocks with the appropriate composition (Simmons *et al*., 1995). More recently, detailed mineralogical and geochemical investigations of pegmatites and experimental studies (for review see Dill, 2015) have led to a significant advance in understanding pegmatite genesis. A full understanding of pegmatite genesis and internal differentiation must extend beyond the paradigm of simple fractionation of parental granite (Dill, 2015). Nonetheless, the massive pegmatites chosen for chemical study here are simpler to interpret than zoned pegmatites and we will test whether the major and trace element co-variations in our data can be interpreted as fractional crystallization trends.

Post-collisional rocks (610–590Ma) are widely distributed in the extreme northern part of the ANS, in the North Eastern Desert and Sinai. They include intrusions of calc-alkaline and alkaline granitoids and their associated volcanics. Determining the tectonic settings of post-collisional granitoids is complicated and it must be recognized that magmas of variable sources and types may be generated (Liégeois *et al*., 1998; Bonin, 2004, 2007); nevertheless, understanding the origin of such rocks has significant geodynamic implications. The pegmatites, aplites and alkali granites of TMC are consistent in field relations and geochemistry with being post-collisional in character (Fig 7A, B, C) and they have characteristics both of A-type granites (Fig. 6C) and highly fractionated calc-alkaline magmas (Fig. 6B). In a post-collisional environment these features may simply represent derivation of magmas from a lithospheric mantle that was previously metasomized by earlier subduction-related processes. This has been

TABLE 2. Contents of REE and ratios in pegmatites, aplite and granite

Rock type	Pegmatites				Aplite		Granite	
	K-rich pegmatite		Na-rich pegmatite					
	PT25	PT34	PT13	PT37	AT21	AT30	GT1	GT4
La	52,8	62,7	38,3	33,1	26,5	27,0	38,0	58,2
Ce	116,1	145,3	94,4	84,0	65,1	68,9	85,5	114,7
Pr	15,29	17,74	10,10	9,57	7,96	8,58	9,97	12,75
Nd	60,9	70,1	37,9	38,0	33,6	31,4	37,3	47,1
Sm	14,80	17,03	7,81	9,26	9,47	8,85	7,80	8,87
Eu	0,40	0,43	0,20	0,19	0,12	0,10	0,86	0,89
Gd	14,00	11,7	7,03	9,23	9,23	8,98	6,63	5,57
Tb	2,35	2,12	1,14	1,59	1,67	1,75	1,12	0,88
Dy	13,65	12,41	6,86	10,26	9,82	11,23	6,33	4,92
Ho	2,74	2,54	1,48	2,27	2,02	2,43	1,27	0,89
Er	7,72	7,41	4,06	6,20	5,98	6,92	3,58	3,09
Tm	1,12	1,09	0,62	0,93	0,91	1,07	0,57	0,47
Yb	6,86	6,94	3,89	5,82	5,75	7,35	3,55	3,31
Lu	0,99	0,93	0,58	0,87	0,81	1,05	0,47	0,46
ΣREE	309,6	358,44	214,3	211,3	179,0	185,6	202,9	262,1
Eu/Eu*	0,08	0,09	0,08	0,06	0,04	0,03	0,36	0,39
(La/Sm)n	2,25	2,32	3,10	2,26	1,77	1,93	3,07	4,14
(Gd/Lu)n	1,73	1,54	1,48	1,30	1,40	1,04	1,73	1,48
(La/Lu)n	5,46	6,91	6,77	3,90	3,35	2,62	8,28	12,96

Eu* = arithmetric $((Sm_N+Gd_N)/2)$
n = chondrite normalized values

recognized in Ediacaran magmatism of the northern ANS (Friz-Topfer, 1991; Iacumin *et al.*, 1998; Kessel *et al.*, 1998; Azer and El-Gharbawy, 2011; Khalil *et al.*, 2015).

Although the pegmatites and aplites of TMC are different in mineralogy and major oxides from the alkali granites in the mapped area, they show similar characteristics in trace and REE patterns, indicating a similar source for all the studied granitoids. On the basis of Essawy *et al.* (1997) suggest a sedimentary source rock for the pegmatites and alkali granites of TMC, but according to Chappell and White (2001) there is substantial overlap between the ASI values of I- and S-type granitoids. Furthermore, the ASI of our samples is near unity (Table 1), which in fact confidently excludes a sedimentary protolith and supports an I-type source (Chappell and White, 1974).

The trace element content of granitic melts change substantially as crystallization proceed and can be used as indicators of magmatic fractionation and chemical evolution of pegmatites (London, 2008). Some element ratios (Rb/Sr, Rb/Ba, Nb/Zr and Y/Nb) show wide variations among pegmatites, aplites and alkali granites (Table 1). This can be attributed to one of the following: i) external sources of Ba and Sr (*e.g.* Charoy *et al.*, 2003), ii) retention of Ba and Sr by fluxed magmas (London *et al.*, 1989) and iii) systematic differences in the partitioning of these elements among plagioclase, K-feldspar and melt (Icenhower and London, 1996). In fact, the systematic variation of some major and trace element contents of the studied rocks (Fig. 8) can be reasonably interpreted in terms of fractional crystallization processes. Decrease of Fe_2O_3, CaO, TiO_2 and P_2O_5 contents with increasing SiO_2 content is consistent with fractionation of apatite and Ti oxides. Significant Sr, Eu and Ba depletions indicate K-feldspar as well as plagioclase fractionation.

Crystallization conditions and depth

Until recently, pegmatites were widely believed to be products of extremely slow cooling, but recent studies show that typically-sized pegmatite bodies likely cooled to their solidus in a few days or months (Chakoumakos and Lumpkin, 1990; Webber *et al.*, 1997, 1999; Morgan and London, 1999). Černý (2005) has more recently suggested that the very large Tanco pegmatite solidified quite rapidly, in decades to a few hundred years. The Taba pegmatites intruded schists and gneisses with little apparent thermal effect. Most of the intrusive contacts parallel the regional foliation of the metamorphic host rocks and only locally cross-cut the regional fabric. The generally conformable contacts and the lack of contact metamorphism around the Taba pegmatites can be taken as evidence for emplacement at mid-crustal depths. This is supported by the presence of miarolitic cavities and the abundance of granitic rocks relative to pegmatitic rocks (London, 2008).

Textural relations in the studied pegmatites indicate that the dominant feature is the virtually contemporaneous nature of the essential minerals. The gross relations between quartz and feldspars suggest that they were formed later than the accessory minerals such as biotite, tourmaline and apatite. Skeletal crystals of beryl can be interpreted as indicating virtually simultaneous crystallization of beryl and the associated minerals. The zoning in some pegmatite lenses in TMC can be attributed to periodic escape of pegmatitic melts, facilitated by volatile influxes. The hypersolvus nature of the studied pegmatites, aplites and alkali granites suggests low water pressure and a high temperature of crystallization, similar to other rocks emplaced at relatively shallow depth (King *et al.*, 1997; Klimm *et al.*, 2003). Unfortunately, the analyzed feldspars cannot be used to estimate the crystallization temperature due to the hypersolvus nature of the rocks and the limited variation in their feldspar compositions.

On the other hand, if all the whole rock compositions in this study are taken as approximations of magmatic liquid compositions, and if the textural indication of contemporaneous quartz and feldspars growth indicates that all the liquids were quartz- and feldspar-saturated, then the pressure dependence of normative quartz content at the ternary granite minimum can be taken as a barometer (Gualda and Ghiorso, 2014). It is impossible for all the rocks in this study to represent quartz and feldspar co-saturated liquids at the same pressure. Although water content and oxygen fugacity, which are nominally free variables, affect the estimate of saturation pressure somewhat, the effects are not large enough to move the cotectic from 73.4wt.% SiO_2, the average value in the alkali granites, to 76.5wt.% SiO_2,

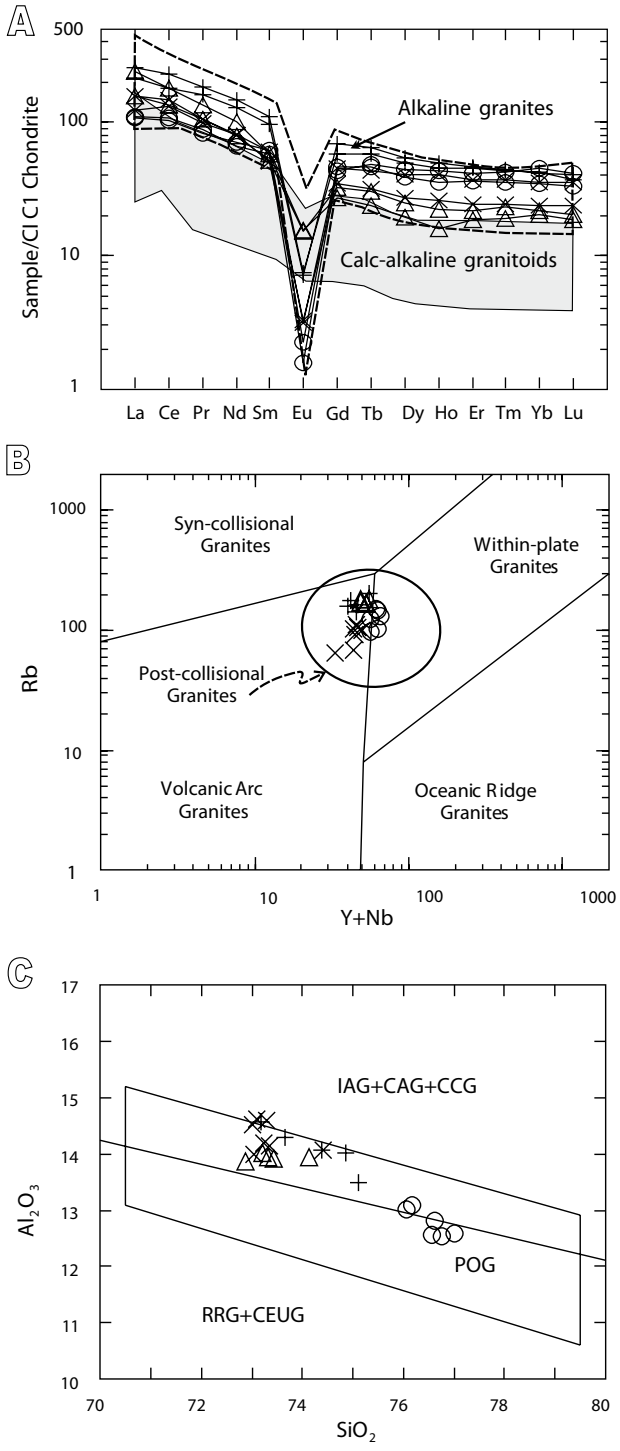

FIGURE 7. TA) Chondrite normalized REE plots for the study samples with normalization values of Evensen *et al.* (1978), compared to post-collisional calc-alkaline and alkaline granitoids in the Arabian-Nubian Shield (ANS) (Eyal *et al.*, 2010; Azer, 2013; Sherif *et al.*, 2013; Azer *et al.*, 2014). B) Rb *vs.* (Y+Nb) diagram of Pearce *et al.* (1984), modified by Pearce (1996). C) Al_2O_3 *vs.* SiO_2 diagram of Maniar and Piccoli (1989). IAG: Island Arc Granitoids, CAG: Continental Arc Granitoids, CCG: Continental Collision Granitoids, POG: Post-Orogenic Granitoids, RRG: Rift-Related Granitoids, CEUG: Continental Epeirogenic Uplift Granitoids. Symbols are as in Figure 6.

the average in the aplites, at constant pressure. Instead, the quantitative SiO_2 barometer of Gualda and Ghiorso (2014) requires that the granites crystallized in the deep crust, near 0.8GPa, and that continuing fractional crystallization was accompanied by ascent through the crust, ending with emplacement of the aplites at the ternary granite minimum in the upper crust, near 0.1GPa. The apparent gradient from the granite crystallization conditions to the aplite crystallization conditions is about 7K/km, indicating a substantially elevated geotherm and rapid ascent with a large component of advective heat transport by the magma.

The contrast in grain size between coarse-grained pegmatite and fine-grained aplites has been the subject of numerous investigations. According to the recent model of pegmatite evolution (London, 2005), water saturation is neither necessary nor likely in the early crystallization of pegmatites, given the combined influence of elements such as B, F, P and Li, in addition to H_2O, in lowering the crystallization temperature, decreasing nucleation rates, decreasing melt polymerization, decreasing viscosity and increasing diffusion rates. As cooling proceeds, the melt becomes supersaturated and ion migration is facilitated over greater distances and promotes the growth of the few nuclei resulting in a coarse-grained final product (Simmons *et al.* 2003; London, 2005). As crystallization proceeds, the liquid becomes progressively enriched in incompatible elements and water. Eventually an aqueous vapor phase is likely to evolve in the final stages of pegmatite crystallization, giving rise to miarolitic cavities and pegmatitic minerals (quartz and feldspars).

The studied aplites are typically thin, low-angle to subhorizontal, sheet-like sills with granitic compositions. The fine grained aplite may result from rapid crystal growth from a highly undercooled granitic melt due to sudden loss of water vapor or pressure-driven quenching. There is some textural evidence in the Taba aplites to support rapid crystal growth rates, such as the presence of skeletal quartz and graphic quartz intergrowth with feldspars.

CONCLUSION

The granitoid rocks intruded into the TMC include alkali granites, pegmatites, and aplites. The pegmatites are distinguished into massive and zoned pegmatites. Massive pegmatites are the most common and are divided into K-feldspar-rich and albite-rich groups. Zoned pegmatites have a quartz core, an intermediate zone rich in K-feldspars and an outer finer grained zone rich in albite.

Bent and broken feldspar twin planes and undulatory extinction in quartz indicate post-magmatic deformation of the pegmatites.

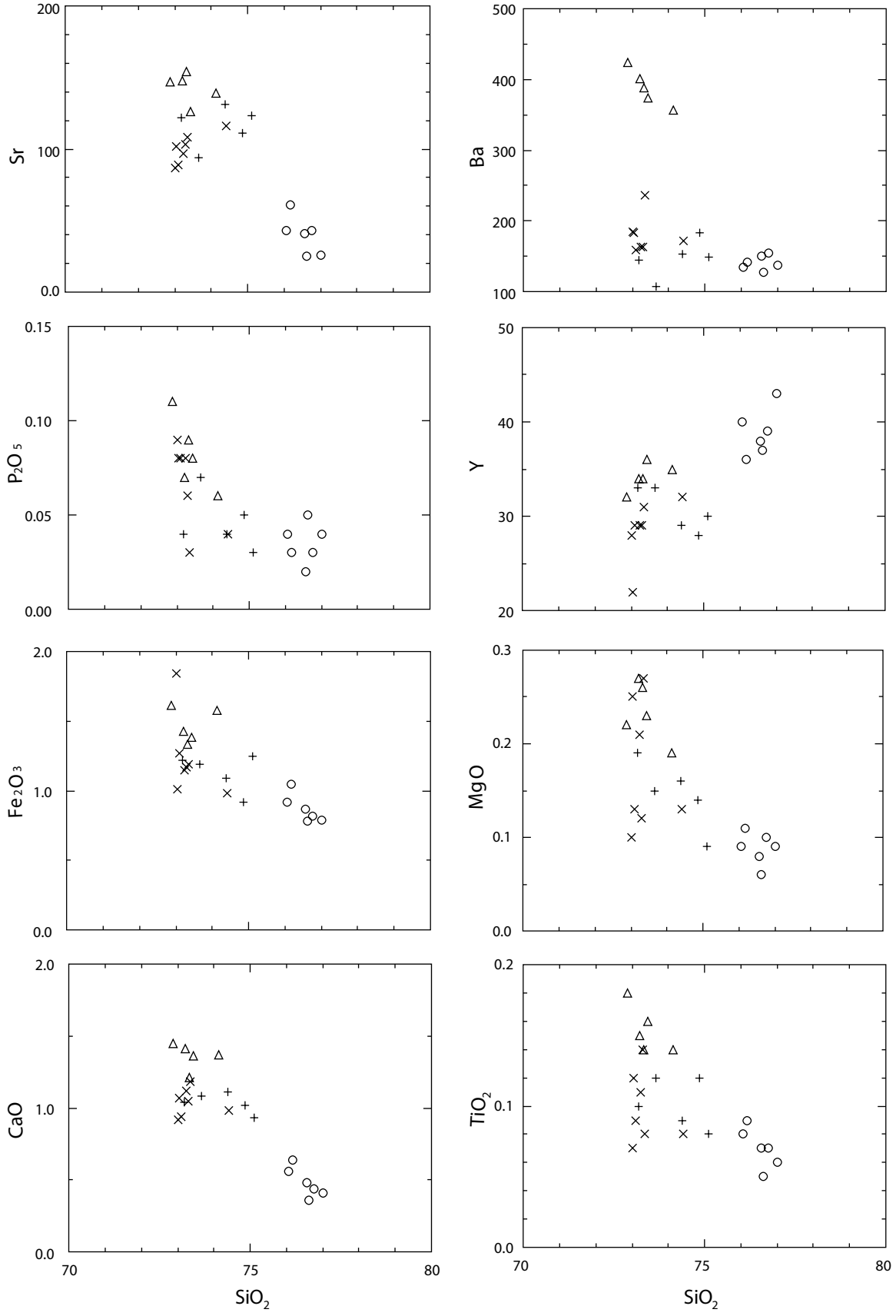

FIGURE 8. SiO_2 variation diagrams of some major and trace elements. Symbols are as in Figure 6.

The studied pegmatites were formed by the intrusion of magmatic fluids into the metamorphic rocks. This is supported by the sharp contacts with the country rocks, structural relations between pegmatites and cross-cutting fracture filling, systematic and progressive changes in the character of certain minerals from outer to inner units; and tapered crystals of beryl that are normal to the pegmatite contact.

There is a clear genetic relation among the alkali granites and pegmatites in the TMC, as indicated by their virtually parallel REE patterns and other geochemical indicators. The pegmatites fractionated and differentiated from the granitic magma and were then injected into foliation and fractures of the metamorphic host rocks. However, if the whole rock compositions indicate liquid compositions that were simultaneously saturated with quartz and feldspars then evolution of the granite magma into the residual aplite magma must have been accompanied by substantial ascent through the crust.

Pegmatites and aplites of the TMC are highly evolved and display geochemical characteristics of post-collisional A-type granites, namely high SiO_2, Na_2O+K_2O, FeO*/MgO, Ga/Al, Zr, Nb, Ga and Y and low CaO, MgO, Ba and Sr. They are rich in REE and have extreme negative Eu anomalies (Eu/Eu*= 0.03–0.09).

ACKNOWLEDGEMENTS

We are indebted to King Saud University, Deanship of Scientific Research, Research Group Nº RG-1436-036, for their support. MKA's visit to the Division of Geological & Planetary Sciences, California Institute of Technology, USA, was supported by the Cairo Initiative of the US Agency for International Development. Special thanks to Prof. George Rossman and Michael Baker for use of sample preparation facilities at Caltech. Also, the authors would like to thank Chi Ma for his help with the microprobe analyses. The authors highly appreciate thoughtful reviews by the Editor (Antonio Castro), Yaron Be'eri-Shlevin and Alexander Falster, which improved the manuscript.

REFERENCES

Abdalla, H.M., El-Afandy, A.H., 2003. Contrasting mineralogical and geochemical characteristics of two A-type pegmatite fields, Eastern Desert Egypt. Egyptian Mineralogist, 15, 287-328.

Abdel-Karim, A.M., 2013. Petrology, geochemistry and petrogenetic aspects of Younger gabbros from south Sinai: a transition from arc to active continental margin. Chemie der Erde, 73, 89-104.

Abu El-Enen, M.M., 2000. Origin of Wadi El-Mahash Younger Granites, SE Sinai, Egypt. In: Abdel Aziz, S.Y. (ed.). Proceedings 5th International Conference Arab World I. Cairo University, 133-148.

Abu El-Enen, M.M., Zalata, A.A., El-Metwally, A.A., Okrusch, M., 1999. Orthogneisses from the Taba metamorphic belt, SE Sinai, Egypt: witnesses for granitoid magmatism at an active continental margin. Neues Jahrbuch Mineralogie Abhandlungen, 175, 53-81.

Abu El-Enen, M.M., Will, T.M., Okrusch, M., 2004. P-T evolution of the Pan-African Taba metamorphic belt, Sinai, Egypt: Constraints from metapelitic mineral assemblages. Journal of African Earth Sciences, 38, 59-78.

Ali, K.A., Azer, M.K., Gahlan, H.A., Wilde, S.A., Samuel, M.D., Stern, R.J., 2010. Age constraints on the formation and emplacement of Neoproterozoioc ophiolites along the Allaqi-Heiani suture, South Eastern Desert of Egypt. Gondwana Research, 18, 583-595.

Avigad, D., Gvirtzman, Z., 2009. Late Neoproterozoic rise and fall of the northern Arabian-Nubian shield: The role of lithospheric mantle delamination and subsequent thermal subsidence. Tectonophysics, 477, 217-228.

Azer, M.K., 2006. The petrogenesis of late Precambrian felsic alkaline magmatism in South Sinai, Egypt. Acta Geologica Polonica, 56, 463-484.

Azer, M.K., 2013. Late Ediacaran (605-580Ma) post-collisional alkaline magmatism in the Arabian-Nubian Shield: a case study of Serbal ring-shaped intrusion, southern Sinai, Egypt. Journal of Asian Earth Sciences, 77, 203-223.

Azer, M.K., El-Gharbawy, R.I., 2011. Contribution to the Neoproterozoic layered mafic-ultramafic intrusion of Gabal Imleih, South Sinai, Egypt: Implication of post-collisional magmatism in the north Arabian-Nubian Shield. Journal of African Earth Sciences, 60, 253-272.

Azer, M.K., Farahat, E.S., 2011. Late Neoproterozoic volcano-sedimentary succession of Wadi Rufaiyil, southern Sinai, Egypt: a case of transition from late- to post-collisional magmatism. Journal of Asian Earth Science, 42, 1187-1203.

Azer, M.K., Stern, R.J., Kimura, J.-I., 2010. Origin of a Late Neoproterozoic (605±13Ma) intrusive carbonate-albitite complex in Southern Sinai, Egypt. International Journal of Earth Sciences, 99, 245-267.

Azer, M.K., Obeid, M.A., Ren, M., 2014. Geochemistry and petrogenesis of late Ediacaran (580-605Ma) post-collisional alkaline rocks from Katherina Ring complex, south Sinai., Egypt. Journal of Asian Earth Sciences, 93, 229-252.

Be'eri-Shlevin, Y., Katzir, Y., Whitehouse, M., 2009. Post-collisional tectono-magmatic evolution in the northern Arabian-Nubian Shield (ANS): Time constraints from ion-probe U-Pb dating of zircon. Journal of Geological Society of London, 166, 71-85.

Be'eri-Shlevin, Y., Samuel, M.D., Azer, M.K., Rämö, O.T., Whitehouse, M.J., Moussa, H.E., 2011. The late Neoproterozoic Ferani and Rutig volcano-sedimentary successions of the northernmost Arabian-Nubian Shield (ANS): New insights from zircon U-Pb geochronology, geochemistry and O-Nd isotope ratios. Precambrian Research, 188, 21-44.

Bentor, Y.K., 1985. The crustal evolution of the Arabo-Nubian Massif with special reference to Sinai Peninsula. Precambrian Research, 28, 1-74.

Bielski, M., 1982. Stages in the evolution of the Arabian-Nubian Massif in Sinai. Ph.D. Thesis. Jerusalem, Hebrew University, 155pp.

Bonin, B., 2004. Do coeval mafic and felsic magmas in post-collisional to within- plate regimes necessarily imply two contrasting, mantle and crustal, sources? A review. Lithos, 78, 1-24.

Bonin, B., 2007. A-type granites and related rocks: Evolution of a concept, problems and prospects. Lithos, 97, 1-29.

Černý, P., 1991. Rare-element granitic pegmatites. Part 1: Anatomy and internal evolution of pegmatite deposits. Part 2: Regional to global environments and petrogenesis. Geoscience Canada, 18, 49-81.

Černý, P., 2005. REE-Enriched Granitic Pegmatites, In: Linnen, R.L., Sampson, I.M. (eds.). Rare-Element Geochemistry and Mineral Deposits. Geological Association of Canada (GAC), Short Course Notes, 17, 175-199.

Černý, P., Ercit, T.S., 2005. Classification of granitic pegmatites revisited. Canadian Mineralogist, 43, 2005-2026.

Chakoumakos, B.C., Lumpkin, G.R., 1990. Pressure-temperature constraints on the crystallization of the Harding pegmatite, Taos County, New Mexico. Canadian Mineralogist, 28, 287-298.

Chappell, B.W., White, A.J.R., 1974. Two contracting granite types. Pacific Geology, 8, 173-174.

Chappell, B.W., White, A.J.R., 2001. Two contrasting granite types: 25 years later. Australian Journal of Earth Sciences, 48, 489-499.

Charoy, B., Chaussidon, M., Le Carlier De Veslud, C., Duthoud, J.L., 2003. Evidence of Sr mobility in and around the albite-lepidolite-topaz granite of Beauvoir (France): an in situ ion and electron probe study of secondary Sr-rich phosphates. Contribution to Mineralogy and Petrology, 145, 673-690.

Cosca, M.A., Shimron, A., Caby, R., 1999. Late Precambrian metamorphism and cooling in the Arabian-Nubian Shield: petrology and $^{40}Ar/^{39}Ar$ geochronology of metamorphic rocks of the Elat area (southern Israel). Precambrian Research, 98, 107-127.

Cox, G., Lewis, C.J., Collins, A.S., Nettle, D., Halverson, G.P., Foden, J., Kattan, F., Jourdan, F., 2012. Ediacaran Terrane accretion in the Arabian Nubian Shield. Gondwana Research, 21, 341-352.

De la Roche, H., Leterrier, J., Grandclaude, P., Marchal, M., 1980. A classification of volcanic and plutonic rocks using R1-R2 diagrams and major-element analyses: Its relation with current nomenclature. Chemical Geology, 29, 183-210.

Deer, W.A., Howie, R.A., Zussman, J., 1992. An introduction to the rock forming minerals. London, Longman Scientific and Technical, Second Edition, 696pp.

Dill, H.G., 2015. Pegmatites and aplites: Their genetic and applied ore geology. Ore Geology Reviews, 69, 417-561.

El-Sheshtawi, Y.A., Aly, M.M., Ahmed, A.M., 1988. Geochemistry and tectonic environments of the granite-pegmatite dykes around Wadi El Marach area, Sinai, Egypt. Mansoura Science Bulletin, 1592, 205-226.

Ercit, T.S., 2004. REE-enriched granitic pegmatites. Rare element geochemistry and ore deposits. In: Linnen, R.L., Samson, I.M. (eds.). Short Course Notes, 17. Geological Association of Canada, 257-296.

Essawy, M.A., El-Metwally, A.A., Althaus, E., 1997. Pan-African layered mafic-ultramafic-mafic cumulate complex in the SW Sinai massif: mineralogy, geochemistry and crustal growth. Chemie der Erde, 57, 137-156.

Evensen, N.M., Hamilton, P.J., O'Nions, R.K., 1978. Rare earth abundances in chondritic meteorites. Geochimica Cosmochimica Acta, 42, 1199-1212.

Eyal, Y., 1980. The geological history of the Precambrian metamorphic rocks between Wadi Twaiba and Wadi UmMara, NE Sinai. Israel Journal of Earth Sciences, 29, 53-66.

Eyal, Y., Amit, O., 1984. The Magrish Migmatites (Northeastern Sinai) and their genesis by metamorphic differentiation triggered by a change in the strain orientation. Israel Journal of Earth Sciences, 33, 188-200.

Eyal, M., Bartov, Y., Shimron, A.E., Bentor, Y.K., 1980. Sinai geological map, aeromagnetic map. Scale: 1:500 000, Survey of Israel, 1 sheet.

Eyal., Y., Eyal., M., Kröner., A., 1991. Geochronology of the Elat Terrain, metamorphic basement, and its implication for crustal evolution of the NE Part of the Arabian-Nubian Shield. Israel Journal of Earth Science, 40, 5-16.

Eyal, M., Litvinovsky, B.A., Katzir, Y., Zanvilevich, A.N., 2004. The Pan-African high- K calc-alkaline peraluminous Elat granite from the southern Israel: geology, geochemistry and petrogenesis. Journal of African Earth Science, 40, 115-136.

Eyal, M., Litvinovsky, B., Jahn, B.M., Zanvilevich, A., Katzir, Y., 2010. Origin and evolution of post-collisional magmatism: coeval Neoproterozoic calc-alkaline and alkaline suites of the Sinai Peninsula. Chemical Geology, 269, 153-179.

Eyal, M., Be'eri-Shlevin, Y., Eyal, Y., Whitehouse, M.J., Litvinovsky, B., 2014. Three successive Proterozoic island arcs in the Northern Arabian-Nubian Shield: Evidence from SIMS U-Pb dating of zircon. Gondwana Research, 25, 338-351.

Farahat, E.S., Azer, M.K., 2011. Post-collisional magmatism in the northern Arabian-Nubian Shield: the geotectonic evolution of the alkaline suite at Gebel Tarbush area, South Sinai, Egypt. Chemie der Erde, 71, 247-266.

Friz-Töpfer, A., 1991. Geochemical characterization of Pan-African dyke swarms in southern Sinai: from continental margin to intraplate magmatism. Precambrian Research, 49, 281-300.

Garfunkel, Z., 1999. History and paleogeography during the Pan-African orogen to stable platform transition: reappraisal of the evidence from the Elat area and the northern Arabian-Nubian Shield. Israel Journal of Earth Sciences, 48, 135-157.

Garfunkel, Z., 2000. The crustal evolution of the Arabo-Nubian massif with special reference to the Sinai Peninsula. Precambrian Research, 28, 1-74.

Ghazaly, M.K., El Afandy, A.H., Fawzy, Kh.M., Fahmy, M.A., 2015. The pegmatitic rocks of El-Hudi and Um Hibal areas, southeastern Desert, Egypt: genesis and petrological characteristics. Arab Journal of Geosciences, 8, 161-186.

Gualda, G.A.R., Ghiorso, M.S., 2014. Phase-equilibrium geobarometers for silicic rocks based on rhyolite-MELTS. Part 1: Principles, procedures, and evaluation of the method. Contribution to Mineralogy and Petrology, 168(1): 1033, 17pp. DOI: 10.1007/s00410-014-1033-3

Iacumin, M., Mazaroli, A., El-Metwally, A.A., Piccirillo, E.M., 1998. Neoproterozoic dyke swarms from southern Sinai (Egypt): geochemistry and petrogenetic aspects. Journal of African Earth Sciences, 26, 49-64.

Icenhower, J., London, D., 1996. Experimental partitioning of Rb, Cs, Sr, and Ba between alkali feldspar and peraluminous melt. American Mineralogist, 81, 719-734.

Jackson, N.J., 1983. Beryl pegmatite at Jabal Tarban, southern Najd region, Kingdom of Saudi Arabia. Journal of African Earth Sciences, 4, 289-291.

Jahns, R.H., Burnham, C.W., 1969. Experimental studies of pegmatite genesis: I. A model for the derivation and crystallization of granitic pegmatites. Economic Geology, 64, 843-864.

Jahn, B.-M., Wu, F.Y., Capdevila, R., Martineau, F., Zhao, Z., Wang, Y., 2001. Highly evolved juvenile granites with tetrad REE patterns: the Woduhe and Baerzhe granite from the Great Xing'an Mountains in NE China. Lithos, 59, 171-198.

Jarrar, G., Baumann, A., Wachendorf, H., 1983. Age determinations in the Precambrian basement of the Wadi Araba area, southwest Jordan. Earth Planetary Science Letters, 63, 292-304.

Kessel, R., Stein, M., Navon, O., 1998. Petrogenesis of late Neoproterozoic dikes in the northern Arabian-Nubian Shield: Implications for the Origin of A-type granites. Precambrian Research, 92, 195-213.

Khalil, A.E.S., Obeid, M.A., Azer, M.K. 2015. Late Neoproterozoic post-collisional mafic magmatism in the Arabian-Nubian Shield: A case study from Wadi El-Mahash gabbroic intrusion in southeast Sinai, Egypt. Journal of African Earth Sciences, 105, 29-46.

King, P.L., White, A.J.R., Chappel, B.W., Allen, C.M., 1997. Characterization and origin of aluminous A-type granites from the Lachlan Fold Belt, southeastern Australia. Journal of Petrology, 38, 371-391.

Klimm, K., Holtz, F., Johannes, W., King, P.L., 2003. Fractionation of metaluminous A-type granites: an experimental study of the Wangrah Suite, Lachlan Fold Belt, Australia. Precambrian Research, 124, 327-341.

Kröner, A., Eyal, M., Eyal, Y., 1990. Early Pan-African evolution of the basement around Elat, Israel, and Sinai Peninsula revealed by single-zircon evaporation dating, and implication for crustal accretion rates. Geology, 18, 545-548.

Lee, S.-G., Asahara, Y., Tanaka, T., Lee, S.R., Lee, T., 2013. Geochemical significance of the Rb-Sr, La-Ce and Sm-Nd isotope systems in A-type rocks with REE tetrad patterns and negative Eu and Ce anomalies: The Cretaceous Muamsa and Weolaksan granites, South Korea. Chemie der Erde, 73, 75-88.

Liégeois, J.P., Black, R., 1987. Alkaline magmatism subsequent to collision in the Pan-African belt of the Adrar des Iforas. In: Fitton, J.G., Upton, B.G.J. (eds.). Alkaline Igneous Rocks. Geological Society, 30 (Special Publication), 30, 381-401.

Liégeois, J.P., Navez, J., Black, R., Hertogen, J., 1998. Contrasting origin of post-collision high-K calc-alkaline and shoshonitic *versus* alkaline and peralkaline granitoids. The use of sliding normalization. Lithos, 45, 1-28.

London, D., 2005. Geochemistry of Alkali and Alkaline Earth Elements in Ore–Forming Granites, Pegmatites, and Rhyolites. In: Linnen, R.L., Sampson, I.M. (eds.). Rare-Element Geochemistry and Mineral Deposits, 175-199.

London, D., 2008. Pegmatites. The Canadian Mineralogist, 10 (Special Publication), 347pp.

London, D., Morgan, G.B.V.I., Hervig, R.L., 1989. Vapor-undersaturated experiments with Macusani glass+H_2O at 200MPa, and the internal differentiation of granitic pegmatites. Contribution to Mineralogy and Petrology, 102, 1-17.

Maniar, P.D., Piccoli, P.M., 1989. Tectonic discrimination of granitoids. Geological Society of American Bulletin, 101, 635-643.

Meert, J.G., 2003. A synopsis of events related to the assembly of eastern Gondwana. Tectonophysics, 362, 1-40.

Morgan, G.B.VI, London, D., 1999. Crystallization of the Little Three layered pegmatite-aplite dike, Ramona District, California. Contributions to Mineralogy and Petrology, 136, 310-330.

Morag, N., Avigad, D., Gerdes, A., Belousova, E., Harlavan, Y., 2011. Crustal evolution and recycling in the northern Arabian-Nubian Shield: new perspectives from zircon Lu-Hf and U-Pb systematics. Precambrian Research, 186, 101-116.

Nachit, H., Ibhi, A., Abia, E.H., Ohoud, M.B., 2005. Discrimination between primary magmatic biotites, reequilibrated biotites and neoformed biotites. Comptes Rendus Géoscience, 337, 1415-1420.

Pallister, J.S., Stacy, J.S., Fisher, L.B., Premo, W.R., 1988. Precambrian ophiolites of Arabia: geological settings, U-Pb geochronology, Pb-isotope characteristics, and implications for crustal accretion. Precambrian Research, 38, 1-54.

Patchett, P.J., Chase, C.G., 2002. Role of transform continental margins in major crustal growth episodes. Geology, 30, 39-42.

Pearce, J.A., 1996. Sources and settings of granitic rocks. Episodes, 19, 120-125.

Pearce, J.A., Harris, N.B.W., Tindle, A.G., 1984. Trace element discrimination diagrams for the tectonic interpretation of granitic rocks. Journal of Petrology, 25, 956-983.

Samuel, M.D., Moussa, H.E., Azer, M.K., 2001a. Geochemistry and petrogenesis of Iqna Shar,a volcanic rocks, Central Sinai, Egypt. Egyptian Journal of Geology, 45(2), 921-940.

Samuel, M.D., Moussa, H.E., Azer, M.K., 2001b. Petrography and mineral chemistry of Iqna Shar,a volcanic rocks , Central Sinai, Egypt. Egyptian Journal of Geology, 45(1), 107-130.

Samuel, M.D., Moussa, H.E., Azer, M.K., 2007. A-type Volcanics in Central Eastern Sinai, Egypt. Journal of African Earth Sciences, 47, 203-226.

Sherif, M.I., Ghoneim, M.F., Heikal, M.T.S., El Dosuky, B.T., 2013. Perogenesis of granites, Sharm El-Sheikh area, South Sinai, Egypt: petrological constrains and tectonic evolution. Mineralogy and Petrology, 107, 765-783.

Shimron, A.E., 1972. The Precambrian Structural and Metamorphic History of the Elat Area, With Comparative Notes on the Geology of the Sinai Peninsula. Ph.D. thesis. Jerusalem, The Hebrew University, 244pp.

Shimron, A.E., 1988. Discussion on the age of the Feiran basement rocks, Sinai: implications for late Precambrian crustal evolution in the northern Arabian-Nubian Shield. Journal of the Geological Society of London, 145, 1033-1035.

Simmons, W.B., Foorf, E.E., Falster, A.U., King, V.T., 1995. Evidence for an anatectic origin of granitic pegmatites, western Maine, USA. Geological Society of America, abstracts with programs, 27(6), A411.

Simmons, W.B., Webber, K.L., Falster, A.U., Nizamoff, J.W., 2003. Pegmatology - Pegmatite Mineralogy, Petrology and Petrogenesis. New Orleans (Lousiana), Rubellite Press, 176pp.

Stein, M., 2003. Tracing the plume material in the Arabian-Nubian Shield. Precambrian Research, 123, 223-234.

Stein, M., Goldstein, S., 1996. From plume head to continental lithosphere in the Arabian-Nubian Shield. Nature, 382, 773-778.

Stern, R.J., 1994. Arc assembly and continental collision in the Neoproterozoic East African Orogen: implications for the consolidation of Gondwanaland. Annual Reviews of Earth and Planetary Science, 22, 319-351.

Stern, R.J., Manton, W.I., 1987. Age of Feiran basement rocks, Sinai: implications for late Precambrian crustal evolution in the northern Arabian-Nubian Shield. London, Journal of the Geological Society, 144, 569-575.

Stoeser, D.W., Frost, C.D., 2006. Nd, Pb, Sr and O isotope characterization of Saudi Arabian Shield terranes. Chemical Geology, 226, 163-188.

Sylvester, P.J., 1989. Post-collisional alkaline granites. Journal of Geology, 97, 261-280.

Webber, K.L., Falster, A.U., Simmons, W.B., Foord, E.E., 1997. The role of diffusion-controlled oscillatory nucleation in the formation of line rock in pegmatite-aplite dikes. Journal of Petrology, 38, 1777-1791.

Webber, K.L., Simmons, W.B., Falster, A.U., Foord, E.E., 1999. Cooling rates and crystallization dynamics of shallow level pegmatite-aplite dikes, San Diego County, California. American Mineralogist, 84, 708-717.

Whalen, J.B., Currie, K.L., Chappel, B.W., 1987. A-type granites: geochemical characteristics, discrimination and petrogenesis. Contribution to Mineralogy and Petrology, 95, 407-419.

Wise, M.A., 1999. Characterization and classification of NYF-type pegmatites. Canadian Mineralogist, 37, 802-803.

Zhao, Z.H., Xiong, X.L., Han, X.D., Wang, Y.X., Wang, Q., Bao, Z.W., Jahn, B.M., 2002. Controls on the REE tetrad effect in granites: evidence from the Qianlishan and Baerzhe granites, China. Geochemical Journal, 36, 527-543.

Manuscript received January 2016;
revision accepted March 2016;
published Online June 2016.

ELECTRONIC APPENDIX I

TABLE I. Microprobe analyses of K-feldspar in the K-rich pegmatites

Sample No.	PT25															
Spot No.	#4	#5	#9	#19	#20	#21	#22	#26	#27	#28	#29	#30	#5	#13	#14	#15
SiO_2	66,24	66,27	66,30	66,04	66,01	65,77	66,12	66,00	65,51	65,73	66,19	65,52	65,82	66,10	66,14	65,18
Al_2O_3	18,67	18,72	18,78	18,60	18,60	18,50	18,59	18,61	18,56	18,57	18,58	18,58	18,51	18,57	18,66	18,47
MgO	0,00	0,00	0,00	0,00	0,00	0,00	0,00	0,00	0,00	0,00	0,00	0,00	0,00	0,00	0,00	0,00
CaO	0,03	0,02	0,04	0,03	0,02	0,20	0,01	0,02	0,06	0,02	0,01	0,04	0,02	0,01	0,03	0,03
MnO	0,01	0,01	0,01	0,01	0,02	0,02	0,02	0,01	0,01	0,01	0,01	0,02	0,01	0,02	0,01	0,01
FeO	0,03	0,01	0,02	0,03	0,03	0,04	0,03	0,03	0,02	0,02	0,03	0,03	0,02	0,02	0,01	0,03
BaO	0,00	0,00	0,00	0,00	0,00	0,00	0,00	0,00	0,00	0,00	0,00	0,00	0,00	0,00	0,00	0,00
Na_2O	1,11	1,04	1,00	0,72	0,99	0,54	0,72	0,74	0,57	0,85	0,82	1,16	0,79	0,81	0,98	0,53
K_2O	15,04	15,19	15,19	15,50	15,23	15,83	15,57	15,56	15,75	15,42	15,46	14,96	15,50	15,50	15,23	15,83
Total:	101,12	101,27	101,34	100,93	100,91	100,89	101,06	100,97	100,48	100,62	101,09	100,30	100,66	101,02	101,06	100,08
End members (mol.-%):																
Or	89,7	90,5	90,7	93,3	90,9	94,2	93,4	93,2	94,5	92,2	92,5	89,3	92,8	92,6	90,9	95,0
Ab	10,1	9,4	9,1	6,6	9,0	4,8	6,6	6,7	5,2	7,7	7,5	10,5	7,1	7,3	8,9	4,8
An	0,2	0,1	0,2	0,1	0,1	1,0	0,0	0,1	0,3	0,1	0,0	0,2	0,1	0,0	0,1	0,1

Sample No.	Sc (PT7)																			
Spot No.	29	30	31	32	34	47	48	49	50	51	67	68	69	70	85	86	87	88	89	90	91
SiO_2	63,98	62,60	62,77	61,52	61,78	64,50	64,81	65,20	63,82	62,96	65,59	66,05	64,40	65,10	65,02	65,20	64,29	65,29	63,66	63,90	64,66
Al_2O_3	18,23	17,78	17,80	17,52	17,62	18,21	18,33	18,30	18,08	17,95	18,07	18,21	18,40	18,35	18,59	18,35	18,85	18,34	18,06	18,09	18,28
MgO	0,00	0,00	0,00	0,00	0,00	0,00	0,00	0,00	0,00	0,00	0,00	0,00	0,02	0,00	0,00	0,00	0,00	0,00	0,00	0,00	0,00
CaO	0,01	0,02	0,01	0,00	0,08	0,01	0,02	0,01	0,00	0,01	0,00	0,01	0,02	0,01	0,02	0,00	0,02	0,02	0,01	0,01	0,05
MnO	0,00	0,00	0,00	0,00	0,02	0,00	0,00	0,00	0,01	0,00	0,00	0,00	0,00	0,00	0,00	0,00	0,00	0,02	0,00	0,02	0,00
FeO	0,23	0,36	0,08	0,16	0,95	0,12	0,15	0,11	0,17	0,14	0,27	0,29	0,21	0,22	0,13	0,29	0,44	0,37	0,15	0,11	0,04
BaO	0,00	0,00	0,00	0,00	0,00	0,00	0,00	0,00	0,00	0,00	0,00	0,00	0,00	0,00	0,00	0,00	0,00	0,00	0,00	0,00	0,00
Na_2O	0,23	0,24	0,25	0,27	0,19	0,24	0,27	0,23	0,23	0,25	0,33	0,27	0,23	0,29	0,30	0,24	0,23	0,25	0,19	0,20	0,14
K_2O	16,36	16,36	16,38	16,30	16,08	16,30	16,22	16,38	16,27	16,38	16,20	16,22	16,21	16,23	16,10	16,24	16,10	16,14	16,34	16,48	16,30
Total:	99,04	97,36	97,30	95,78	96,73	99,39	99,80	100,24	98,58	97,69	100,47	101,05	99,50	100,21	100,16	100,33	99,93	100,43	98,41	98,81	99,48
End members (mol.-%):																					
Or	97,9	97,7	97,7	97,5	97,8	97,7	97,5	97,9	97,9	97,7	97,0	97,5	97,8	97,3	97,2	97,8	97,8	97,6	98,2	98,2	98,4
Ab	2,1	2,2	2,2	2,5	1,8	2,2	2,4	2,1	2,1	2,2	3,0	2,4	2,1	2,6	2,7	2,2	2,1	2,3	1,7	1,8	1,3
An	0,1	0,1	0,1	0,0	0,4	0,1	0,1	0,0	0,0	0,1	0,0	0,0	0,1	0,1	0,1	0,0	0,1	0,1	0,0	0,1	0,3

TABLE II. Microprobe analyses of K-feldspar in the Na-rich pegmatites

Sample No.	PT13																
Spot No.	#12	#13	#16	#33	#2	#3	#6	#7	#14	#1	#4	#5	#7	#9	#11	#12	#14
SiO_2	64,38	64,33	64,25	64,36	64,33	64,45	64,42	64,35	64,38	64,38	64,27	64,34	64,43	64,36	64,36	64,35	64,33
Al_2O_3	18,27	18,29	18,27	18,25	18,27	18,25	18,21	18,20	18,26	18,29	18,35	18,42	18,26	18,29	18,30	18,29	18,30
MgO	0,00	0,00	0,00	0,00	0,00	0,00	0,00	0,00	0,00	0,00	0,00	0,01	0,00	0,00	0,00	0,00	0,00
CaO	0,02	0,03	0,02	0,03	0,02	0,03	0,03	0,02	0,02	0,03	0,03	0,03	0,02	0,02	0,02	0,02	0,03
MnO	0,01	0,01	0,02	0,01	0,01	0,01	0,01	0,01	0,01	0,01	0,01	0,01	0,01	0,01	0,01	0,01	0,02
FeO	0,14	0,14	0,11	0,13	0,17	0,11	0,12	0,12	0,11	0,28	0,25	0,13	0,11	0,12	0,13	0,12	0,15
BaO	0,00	0,00	0,00	0,00	0,00	0,00	0,00	0,00	0,00	0,00	0,00	0,00	0,00	0,00	0,00	0,00	0,00
Na_2O	0,76	0,88	0,75	0,83	0,79	0,72	0,74	0,90	0,68	0,68	0,73	0,49	0,74	0,63	0,61	0,61	0,70
K_2O	15,38	15,19	15,32	15,28	15,26	15,41	15,39	15,17	15,47	15,43	15,31	15,70	15,38	15,53	15,55	15,59	15,43
Total:	98,97	98,86	98,74	98,88	98,84	98,97	98,91	98,77	98,92	99,10	98,94	99,13	98,94	98,95	98,98	98,99	98,96
End members (mol.-%):																	
Or	92,9	91,8	93,0	92,2	92,6	93,3	93,1	91,6	93,6	93,6	93,1	95,3	93,1	94,1	94,2	94,3	93,4
Ab	6,9	8,1	6,9	7,6	7,3	6,6	6,8	8,3	6,3	6,3	6,7	4,5	6,8	5,8	5,7	5,6	6,5
An	0,1	0,2	0,1	0,2	0,1	0,1	0,1	0,1	0,1	0,1	0,2	0,2	0,1	0,1	0,1	0,1	0,1

TABLE III. Microprobe analyses of K-feldspar in the Na-rich pegmatites

Sample No.	AT38											
Spot No.	#1	#12	#13	#21	#17	#19	#24	#26	#34	#39	#42	#44
SiO_2	65,11	65,01	64,85	64,50	64,67	65,35	64,47	64,81	64,69	64,45	64,51	64,56
Al_2O_3	18,50	18,32	18,32	18,38	18,27	18,41	18,36	18,40	18,44	18,32	18,34	18,33
MgO	0,00	0,00	0,00	0,00	0,00	0,00	0,00	0,00	0,00	0,00	0,00	0,00
CaO	0,04	0,05	0,05	0,05	0,07	0,05	0,06	0,07	0,06	0,07	0,06	0,06
MnO	0,00	0,00	0,00	0,00	0,00	0,00	0,00	0,00	0,01	0,01	0,00	0,00
FeO	0,13	0,14	0,20	0,11	0,08	0,10	0,13	0,10	0,12	0,11	0,09	0,15
BaO	0,00	0,00	0,00	0,00	0,00	0,00	0,00	0,00	0,00	0,00	0,00	0,00
Na_2O	1,33	1,38	1,45	1,13	1,24	1,25	1,14	1,60	1,39	1,13	1,20	1,50
K_2O	15,08	14,99	14,94	15,28	15,16	15,20	15,33	14,58	14,87	15,30	15,18	14,87
Total:	100,20	99,89	99,81	99,45	99,48	100,37	99,49	99,56	99,57	99,39	99,37	99,47
Cations (O=8)												
End members (mol.-%):												
Or	88,0	87,5	86,9	89,7	88,7	88,7	89,5	85,4	87,3	89,6	89,0	86,5
Ab	11,8	12,2	12,8	10,1	11,0	11,0	10,2	14,2	12,4	10,1	10,7	13,2
An	0,2	0,2	0,3	0,3	0,3	0,2	0,3	0,3	0,3	0,4	0,3	0,3

TABLE IV. Microprobe analyses of plagioclases in the K-rich pegmatites

Sample No.	PT13															
Spot no.	#16	#17	#18	#13	#41	#42	#43	#44	#45	#55	#56	#57	#77	#78	#84	#85
SiO_2	64.42	64.03	64.36	64.12	64.35	64.28	64.24	64.20	64.28	64.16	64.09	64.37	64.37	64.17	64.10	67.96
Al_2O_3	21.76	22.09	21.87	21.97	21.78	21.76	21.88	21.86	21.86	21.74	21.69	21.66	21.80	21.75	21.85	19.60
MgO	0.00	0.00	0.00	0.00	0.00	0.00	0.00	0.00	0.00	0.00	0.00	0.00	0.00	0.00	0.00	0.00
CaO	3.03	3.12	3.14	3.24	3.03	3.07	3.13	3.11	3.12	3.09	3.10	2.95	3.07	3.07	3.18	0.38
MnO	0.01	0.02	0.02	0.03	0.02	0.02	0.01	0.01	0.02	0.01	0.01	0.02	0.01	0.02	0.01	0.00
FeO	0.07	0.06	0.04	0.07	0.05	0.05	0.04	0.06	0.05	0.11	0.11	0.06	0.07	0.05	0.05	0.03
BaO	0.00	0.00	0.00	0.00	0.00	0.00	0.00	0.00	0.00	0.00	0.00	0.00	0.00	0.00	0.00	0.00
Na_2O	10.05	9.92	9.97	9.91	9.99	9.93	9.93	9.92	9.96	9.96	10.08	10.09	9.99	10.03	9.93	11.70
K_2O	0.20	0.22	0.23	0.23	0.20	0.24	0.23	0.27	0.23	0.22	0.24	0.19	0.21	0.21	0.21	0.09
Total:	99.54	99.46	99.62	99.57	99.41	99.34	99.47	99.43	99.52	99.29	99.31	99.33	99.52	99.30	99.32	99.75
End members (mol.-%):																
Or	1.1	1.2	1.3	1.3	1.1	1.3	1.3	1.5	1.3	1.2	1.3	1.1	1.1	1.1	1.1	0.5
Ab	84.8	84.1	84.1	83.6	84.7	84.3	84.1	84.0	84.2	84.3	84.4	85.2	84.5	84.6	84.0	97.7
An	14.1	14.6	14.6	15.1	14.2	14.4	14.6	14.6	14.6	14.4	14.3	13.7	14.4	14.3	14.9	1.8

Sample No.	Sc (PT7)													
Mineral	Albite													
Spot No.	65	66	71	72	73	74	75	76	77	78	79	80	81	92
SiO_2	69,61	68,88	68,19	69,35	69,27	68,62	69,19	69,55	67,98	69,52	67,46	66,52	66,88	69,14
Al_2O_3	19,29	19,36	19,55	19,59	19,14	19,12	19,23	19,53	19,23	19,33	19,03	19,09	19,01	19,29
MgO	0,00	0,00	0,00	0,00	0,00	0,00	0,00	0,00	0,00	0,00	0,00	0,00	0,00	0,00
CaO	0,02	0,05	0,16	0,07	0,01	0,03	0,01	0,02	0,54	0,02	0,01	0,05	0,05	0,03
MnO	0,00	0,00	0,01	0,00	0,00	0,01	0,01	0,00	0,00	0,00	0,00	0,00	0,01	0,03
FeO	0,30	0,27	0,18	0,21	0,30	0,36	0,20	0,14	0,35	0,23	0,29	0,43	0,16	0,23
BaO	0,00	0,00	0,00	0,00	0,00	0,00	0,00	0,00	0,00	0,00	0,00	0,00	0,00	0,00
Na_2O	11,89	11,80	11,69	11,93	11,73	11,78	11,80	11,61	11,42	11,67	11,79	11,49	11,71	11,76
K_2O	0,06	0,08	0,09	0,06	0,06	0,12	0,07	0,06	0,09	0,08	0,07	0,05	0,05	0,05
Total:	101,17	100,43	99,86	101,20	100,52	100,04	100,52	100,91	99,61	100,84	98,66	97,64	97,88	100,53
End members (mol.-%):														
Or	0,3	0,4	0,5	0,3	0,4	0,7	0,4	0,4	0,5	0,4	0,4	0,3	0,3	0,3
Ab	99,6	99,3	98,8	99,3	99,6	99,2	99,5	99,5	97,0	99,5	99,6	99,5	99,5	99,6
An	0,1	0,2	0,7	0,3	0,1	0,1	0,0	0,1	2,6	0,1	0,1	0,2	0,2	0,1

TABLE V. Microprobe analyses of plagioclases in the Na-rich pegmatites

Sample No.	PT13															
Spot no.	#16	#17	#18	#13	#41	#42	#43	#44	#45	#55	#56	#57	#77	#78	#84	#85
SiO_2	64.42	64.03	64.36	64.12	64.35	64.28	64.24	64.20	64.28	64.16	64.09	64.37	64.37	64.17	64.10	67.96
Al_2O_3	21.76	22.09	21.87	21.97	21.78	21.76	21.88	21.86	21.86	21.74	21.69	21.66	21.80	21.75	21.85	19.60
MgO	0.00	0.00	0.00	0.00	0.00	0.00	0.00	0.00	0.00	0.00	0.00	0.00	0.00	0.00	0.00	0.00
CaO	3.03	3.12	3.14	3.24	3.03	3.07	3.13	3.11	3.12	3.09	3.10	2.95	3.07	3.07	3.18	0.38
MnO	0.01	0.02	0.02	0.03	0.02	0.02	0.01	0.01	0.02	0.01	0.01	0.02	0.01	0.02	0.01	0.00
FeO	0.07	0.06	0.04	0.07	0.05	0.05	0.04	0.06	0.05	0.11	0.11	0.06	0.07	0.05	0.05	0.03
BaO	0.00	0.00	0.00	0.00	0.00	0.00	0.00	0.00	0.00	0.00	0.00	0.00	0.00	0.00	0.00	0.00
Na_2O	10.05	9.92	9.97	9.91	9.99	9.93	9.93	9.92	9.96	9.96	10.08	10.09	9.99	10.03	9.93	11.70
K_2O	0.20	0.22	0.23	0.23	0.20	0.24	0.23	0.27	0.23	0.22	0.24	0.19	0.21	0.21	0.21	0.09
Total:	99.54	99.46	99.62	99.57	99.41	99.34	99.47	99.43	99.52	99.29	99.31	99.33	99.52	99.30	99.32	99.75
End members (mol.-%):																
Or	1.1	1.2	1.3	1.3	1.1	1.3	1.3	1.5	1.3	1.2	1.3	1.1	1.1	1.1	1.1	0.5
Ab	84.8	84.1	84.1	83.6	84.7	84.3	84.1	84.0	84.2	84.3	84.4	85.2	84.5	84.6	84.0	97.7
An	14.1	14.6	14.6	15.1	14.2	14.4	14.6	14.6	14.6	14.4	14.3	13.7	14.4	14.3	14.9	1.8

TABLE VI. Microprobe analyses of plagioclases in the aplite

Sample No.	AT38			
Spot no.	#11	#16	#23	#37
SiO_2	63.32	62.56	62.97	62.69
Al_2O_3	22.68	23.26	23.37	23.21
MgO	0.00	0.00	0.00	0.00
CaO	4.12	4.83	4.74	4.69
MnO	0.01	0.00	0.00	0.01
FeO	0.08	0.07	0.07	0.08
BaO	0.00	0.00	0.00	0.00
Na_2O	9.23	8.85	9.04	9.08
K_2O	0.40	0.34	0.33	0.34
Total:	99.85	99.91	100.52	100.10
End members (mol.-%):				
Or	2.2	1.9	1.8	1.9
Ab	78.4	75.4	76.1	76.3
An	19.3	22.7	22.0	21.8

TABLE VII. Microprobe analyses of biotite in the aplite and Na-rich pegmatites

Rock type	Aplite							Na-rick pegmatite						
Sample No.	AT38							PT13						
Analysis	#15	#3	#33	#36	#41	#48	#5	#11	#12	#36	#37	#38	#39	#9
SiO_2	32,342	31,785	32,332	32,834	33,267	32,99	31,983	35,892	36,116	36,025	36,189	36,109	35,909	36,205
TiO_2	3,855	3,847	3,668	3,715	3,791	3,709	3,969	2,771	2,783	3,116	3,049	3,063	3,081	3,023
Al_2O_3	13,012	13,348	13,204	13,173	13,244	13,322	12,961	16,031	16,121	15,854	15,986	15,956	15,969	15,954
Cr_2O_3	0,001	0,001	0,014	0,003	0,01	0,008	0,001	0	0	0	0	0	0	0
FeO	29,21	29,881	29,68	29,284	29,065	29,199	29,204	18,509	18,562	18,743	18,427	18,384	18,566	18,461
MnO	0,385	0,368	0,335	0,44	0,441	0,447	0,453	0,63	0,626	0,627	0,641	0,643	0,643	0,652
MgO	5,233	5,534	5,365	5,383	5,293	5,116	5,151	9,725	9,275	9,325	9,494	9,533	9,343	9,549
CaO	0,039	0,371	0,047	0,039	0,026	0,084	0,06	0,027	0,027	0,025	0,025	0,017	0,023	0,019
Na_2O	0,132	0,138	0,151	0,153	0,178	0,166	0,152	0,063	0,042	0,082	0,081	0,085	0,083	0,063
K_2O	8,704	7,042	8,217	8,265	8,701	8,41	8,54	8,542	9,16	9,163	9,192	9,241	9,211	9,23
P_2O_5	0	0	0	0,078	0,001	0,023	0,05	0,039	0	0	0,015	0,005	0,016	0,005
F	0,014	0	0,009	0,071	0,021	0,071	0,024	0,335	0,335	0,635	0,325	0,352	0,317	0,228
Cl	0,016	0,055	0,047	0,088	0,024	0,082	0,093	0,216	0,161	0,285	0,156	0,172	0,181	0,183
SO_2	0,006	0,008	0,01	0,036	0,011	0,038	0,064	0	0,045	0,059	0,021	0,045	0,037	0,034
ZrO_2	0	0	0	0,142	0,098	0,13	0	0,125	0,085	0,13	0,055	0,063	0,075	0,06
HfO_2	0,029	0,02	0	0	0	0	0	0	0,01	0	0	0,004	0,002	0,004
Total	92,978	92,398	93,079	93,704	94,171	93,795	92,705	92,905	93,348	94,069	93,656	93,672	93,456	93,67